The interplay between wetting and phase behaviour in binary polymer films and wedges: Monte Carlo simulations and mean field calculations

2005 J. Phys.: Condens. Matter 17 S333

(http://iopscience.iop.org/0953-8984/17/9/005)

INSTITUTE OF PHYSICS PUBLISHING JOURNAL OF PHYSICS: CONDENSED MATTER

J. Phys.: Condens. Matter **17** (2005) S333–S361 doi:10.1088/0953-8984/17/9/005

The interplay between wetting and phase behaviour in binary polymer films and wedges: Monte Carlo simulations and mean field calculations

M Müller and K Binder

Institut für Physik, WA331, Johannes Gutenberg-Universität, D-55099 Mainz, Germany

Received 24 November 2004
Published 18 February 2005
Online at stacks.iop.org/JPhysCM/17/S333

Abstract

By confining a binary mixture, one can profoundly alter its miscibility behaviour. The qualitative features of miscibility in confined geometry are rather universal and are shared by polymer mixtures as well as small molecules, but the unmixing transition in the bulk and the wetting transition are typically well separated in polymer blends. We study the interplay between wetting and miscibility of a symmetric polymer mixture via large scale Monte Carlo simulations in the framework of the bond fluctuation model and via numerical self-consistent field calculations. The film surfaces interact with the monomers via short-ranged potentials, and the wetting transition of the semi-infinite system is of first order. It can be accurately located in the simulations by measuring the surface and interface tensions and using Young's equation.

If both surfaces in a film attract the same component, capillary condensation occurs and the critical point is close to the critical point of the bulk. If surfaces attract different components, an interface localization/delocalization occurs which gives rise to phase diagrams with two critical points in the vicinity of the pre-wetting critical point of the semi-infinite system. The crossover between these two types of phase diagrams as a function of the surface field asymmetry is studied.

We investigate the dependence of the phase diagram on the film width Δ for antisymmetric surface fields. Upon decreasing the film width the two critical points approach the symmetry axis of the phase diagram, and below a certain width, Δ_{tri}, there remains only a single critical point at symmetric composition. This corresponds to a second order interface localization/delocalization transition even though the wetting transition is of first order. At a specific film width, Δ_{tri}, tricritical behaviour is found.

The behaviour of antisymmetric films is compared with the phase behaviour in an antisymmetric double wedge. While the former is the analogy of the wetting transition of a planar surface, the latter is the analogy of the filling behaviour of a single wedge. We present evidence for a second order interface localization/delocalization transition in an antisymmetric double wedge and

relate its unconventional critical behaviour to the predictions of Parry *et al* (1999 *Phys. Rev. Lett.* **83** 5535) for wedge filling. The critical behaviour differs from the Ising universality class and is characterized by strong anisotropic fluctuations. We present evidence that the transition in large double wedges can be of second order although there is a first order wetting transition on a planar substrate.

(Some figures in this article are in colour only in the electronic version)

1. Introduction

By confining a binary mixture, one can profoundly alter its miscibility behaviour [1–7]. The phase behaviour of AB mixtures in pores, slits and films has attracted abiding interest from both theorists and experimentalists [6, 8, 9] alike. For instance, thin polymer films find application in optical lithography used in semiconductor industry. For this specific application polymer bilayers [10, 11], consisting of a thin top-layer (several 10 nm) on a sub-layer, are prepared. The wetting behaviour of the thin film on the sub-layer is of crucial importance for the development of polymer structures after light exposure. We study the interplay between (pre-)wetting and equilibrium phase behaviour by self-consistent field (SCF) theory [12, 13] and Monte Carlo (MC) simulations [14–16]. In particular, we focus on situations where the surfaces attract different components of the mixture.

The qualitative features of the miscibility in confined geometry are rather universal and are shared by polymer mixtures as well as small molecules. Symmetric binary polymer blends are, however, particularly well suited to study the interplay between wetting and miscibility:

(i) The wetting transition temperature typically is much lower than the critical temperature, where demixing occurs in the bulk [14].
(ii) Fluctuations can be controlled by the degree of interdigitation [13, 17]: the more extended the molecule is, the larger is the number of neighbours it interacts with, and the smaller is the effect of fluctuations. Therefore SCF calculations provide an accurate description for many properties except for the ultimate vicinity of critical points. The reduction of fluctuation effects not only applies to composition fluctuations in the vicinity of the critical point, which can be quantified by the Ginzburg criterion [18], but also to interface fluctuations which are pertinent to the wetting behaviour. The spatial extension of the molecules also sets the length scale of enrichment layers and facilitates experimental investigations. Indeed, wetting transitions have been studied in recent experiments [8, 9, 19, 20].
(iii) The vapour pressure of polymer films is vanishingly small, hence the effects of evaporation can be neglected.
(iv) Polymers tend not to crystallize easily. Therefore, wetting phenomena might not be preempted by crystal phases. Likewise there is no roughening transition of the interface at temperature T_R as occurs in Ising-like models. In the latter models only the temperature range $T_c > T > T_R$ is available for studies of the wetting behaviour, and it might be difficult to separate bulk-like fluctuations of the order parameter from interface fluctuations.

Using a coarse-grained polymer [17, 21] model for an AB binary melt we locate the first order wetting transition, the phase diagram in a symmetric slit pore (symmetric film) [14], and the phase diagram in a thin film where the substrate favours the A-component of the mixture with the same strength as the top surface attracts the B-component (antisymmetric film) [13, 15].

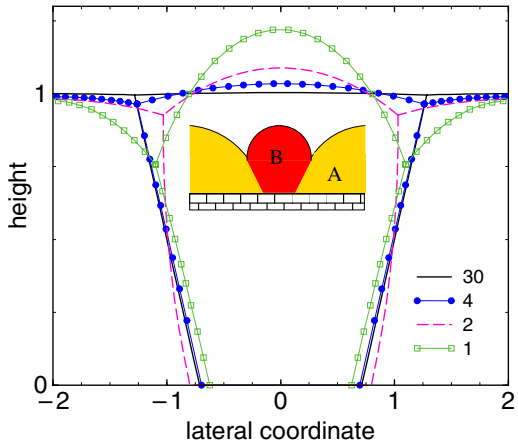

Figure 1. Laterally segregated binary film. The shape of the interfaces is obtained by minimizing the effective Hamiltonian $H = \gamma_{AB}L_{AB} + \gamma_{AS}L_{AS} + \gamma_{BS}L_{BS} + \gamma_{AV}L_{AV} + \gamma_{BV}L_{BV}$ at fixed volume of the components. L_{ij} denotes the area of the interface between substances i and j, and γ_{ij} the corresponding interface tension. We assume that the interface positions do not vary in the direction perpendicular to the lateral coordinate shown, i.e., cylindrical domain shapes. The figure refers to the choice $\gamma_{AV} - \gamma_{BV} = \gamma_{AS} - \gamma_{BS} = 0.5\gamma_{AB}$, $\gamma_{BS} = \gamma_{AB}$ and γ_{AV}/γ_{AB} as indicated in the key. From [26].

Then, we discuss the phase behaviour in a quadratic pore where two neighbouring surfaces favour the A-component and the other two neighbouring surfaces favour the B-component (antisymmetric double wedge) [22, 23]. We conclude with an outlook.

2. Model and techniques

We consider a binary polymer blend. Both species—A and B—contain the same number N of monomers per chain and have the same spatial extension R_e. They are confined into a thin film; the bottom substrate (W) might be a silicon wafer, while the other surface might be the interface to the vapour (vacuum, V). In general, a compressible mixture of two polymers exhibits a quite rich phase diagram [24, 25]. In addition to liquid–liquid demixing into an A-rich and a B-rich liquid, there occur liquid vapour coexistence regions and also liquid–liquid–vapour three-phase regions. The case of a partially miscible binary polymer blend on a solid support corresponds to liquid–liquid–vapour coexistence. Depending on the ratio of the interface tension γ_{AB} between the segregated bulk phases and the surface tension γ_{AV}, γ_{BV} of the components and the vapour, the upper surface might be rough. The qualitative behaviour is illustrated in figure 1, where we obtain the shape of the segregated domains by minimizing the sum of the interface and surface free energies at constant volume of the coexisting phases. If the AB interface tension is comparable to the liquid/vapour tension, it 'drags' the film surface towards the substrate so as to reduce the length of the AB interface. A rather rich morphology of droplets and wetting patterns can be expect in compressible binary mixtures [27]. If the liquid/vapour tension exceeds the AB interface tension by about two orders of magnitude, however, the surface is almost flat, and the situation is equivalent to a binary mixture between two hard surfaces a distance Δ apart [26]. In the following we shall restrict ourselves for simplicity to this case, $\gamma_{AB} \ll \gamma_{AV}$ or γ_{BV}. In this limit, the liquid–vapour interface resembles the interface between the polymer and the substrate, i.e., both interfaces are much narrower than the AB interface between the A-rich and B-rich liquid. Then, the behaviour of a supported

binary film is similar to the behaviour of a binary mixture confined into a rigid, slit-like pore[1] [28].

2.1. Monte Carlo (MC) simulations

In the MC simulations we use a computationally efficient, coarse-grained lattice model. The bond fluctuation model [17, 21] retains the universal features of polymers—connectivity, excluded volume of segments and a thermal interaction which leads to phase separation—but ignores details of chemical structure. Effective monomers prevent the corners of a unit cell of a 3D cubic lattice from double occupancy. We use chain length $N = 32$. Monomers along a chain are connected via bond vectors of length 2, $\sqrt{5}$, $\sqrt{6}$, 3 or $\sqrt{10}$ in units of the lattice spacing u. The end-to-end distance of the chains is given by $R_e(N = 32) \approx 17u$, and it is almost independent of temperature. The simulations are performed at a monomer number density of $\Phi = 1/16$. This density corresponds to a concentrated solution or melt, where the chains adopt Gaussian conformations on large length scales. Different monomers repel each other by a square well potential of depth ϵ which comprises the nearest 54 neighbours up to a distance $\sqrt{6}u$; like monomers attract each other. The strength of the repulsion is proportional to the Flory–Huggins parameter $\chi = 5.3\epsilon/k_BT$ [17]. The surfaces are structureless and impenetrable. They act on monomers in the two nearest layers ($d_{wall} = 2$) with strength ϵ_{wall} (short-ranged surface forces). A positive value corresponds to an attraction to A-monomers. For thin films we use $\epsilon_{wall} = 0.16k_BT$.

This coarse-grained model is well-suited to investigating the interplay of wetting and phase separation in binary polymer mixtures or collective phenomena in self-assembled systems [29]. On the one hand, one expects that details of the atomistic structure of the polymers influence the statistical mechanics on larger, mesoscopic length scales only via a small number of coarse-grained parameters, e.g., the incompatibility between the two polymer species, χN, the length scale given by the end-to-end distance, R_e, and the invariant degree of polymerization, $\bar{N} = (\Phi R_e^3/N)^2$, which parameterizes the strength of fluctuation effects. We can assess the validity of this expectation and explore the role of fluctuations by quantitatively comparing the results of the MC simulations and the SCF theory. On the other hand, a segment of the coarse-grained model corresponds to a small number of repeat units on the atomistic scale. The reduction in the number of degrees of freedom and, more importantly, the simplifications and softening of the interaction potential between the coarse-grained segments are necessary to explore the phenomena on large length and time scales pertinent to the wetting and phase behaviour. Note that in the following we use system sizes with up to 2.8 million lattice sites.

The MC simulations are performed in the semi-grandcanonical ensemble, i.e., we fix the incompatibility/temperature, the volume, the total number of polymers, and the chemical potential difference $\Delta\mu$ between the two species, but the composition of the melt fluctuates. The simulations comprise two types of MC moves. Canonical moves relax the conformations of the polymer on the lattice, but leave the composition unaltered. We use random, local monomer displacements and slithering snake movements. The semi-grandcanonical moves consist of relabelling an A-polymer into a B-polymer and vice versa [30]. This MC move changes the composition but leaves the polymer conformations unaltered. Of course, these moves are greatly facilitated by the structural symmetry of the polymer species, although they can also be applied to polymers that differ in their stiffness [31] or chain length [32].

The key quantity to be monitored in the simulation is the probability distribution P of the composition ϕ. In the vicinity of phase coexistence, $P(\phi)$ exhibits a two-peak structure,

[1] If the film surfaces are elastic (mechanically confined) as opposed to strictly rigid, the interplay between phase separation and elastic distortion of the surfaces gives rise to interesting pattern formation (see [28]).

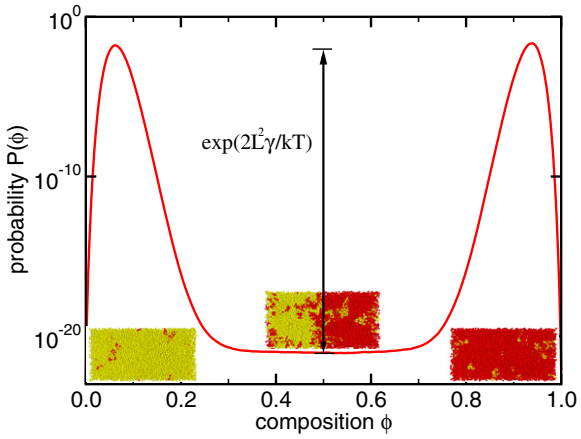

Figure 2. Probability distribution of the composition at $\epsilon = 0.02 k_B T$ (i.e., $T/T_c^{bulk} = 0.7215$) in a system of geometry $3.8R_e \times 3.8R_e \times 7.5R_e$ with periodic boundary conditions in all three directions. The two peaks correspond to the A-rich and the B-rich phase as indicated by the snapshots. Around $\phi = 1/2$ the typical configuration consists of two domains separated by two AB interfaces of size L^2. It is advantageous to use an elongated simulation cell [33]: the slab configuration—an A-rich domain that spans the simulation cell in the two shorter directions and is separated by two interfaces from a B-rich domain—is stable over a larger range of composition and for symmetric composition, $\phi = 1/2$, the two AB interfaces are further apart, thereby reducing the interactions between the two interfaces.

as can be seen in figure 2. The location of the coexistence can be accurately determined by the equal weight criterion [34]. For the system to explore the pertinent range of compositions and to establish that it spends equal amount of time in both phases, the system has to tunnel often between the two peaks in the course of the simulation. Typically, the two phases are, however, separated by a large free energy barrier, which corresponds to the free energy cost of two interfaces between the coexisting phases of size L^2 (L being the linear dimension of the simulation cell). In order to facilitate tunnelling between the different regions in configuration space that correspond to the different phases, we employ a re-weighting technique. To this end one adds a weighting function $k_B T \ln w(\phi)$ to the Hamiltonian, that depends only on the average composition ϕ of the system, but not on the details of the configurations [35]. If one chooses $w(\phi) \approx P(\phi)$ the system will sample all compositions with roughly equal probability. A suitable estimate of $P(\phi)$ can be generated by histogram extrapolation [36], starting in the vicinity of the critical point where the two phases are not separated by a large free energy barrier. Other methods, e.g., the Wang–Landau algorithm [37] or successive umbrella sampling [38], have also been employed. This method allows us to determine phase coexistence in the bulk and in confined geometry, and it additionally provides information about the interface and surface tension, $\gamma_{AB} = \frac{k_B T}{2L^2} \ln P_{max}/P_{min}$ [39]. These techniques can also be applied to determine the difference of the surface free energies from the simulations or to wetting transitions of one-component polymer solutions [40–42] and Ising models [23].

2.2. *Self-consistent field (SCF) calculations*

Additionally, we calculate the phase behaviour of a confined AB mixture within the SCF theory of Gaussian polymers [43–45]. The film comprises a volume $V_0 = \Delta_0 \times L \times L$. Δ_0 denotes the film width, while L is the lateral extension of the film. The density at the film surfaces

decreases to zero in a boundary region of width Δ_w according to [46]

$$\Phi_0(x) = \begin{cases} \dfrac{1-\cos\left(\frac{\pi x}{\Delta_w}\right)}{2}; & 0 \leqslant x \leqslant \Delta_w \\ 1; & \Delta_w \leqslant x \leqslant \Delta_0 - \Delta_w \\ \dfrac{1-\cos\left(\frac{\pi(\Delta_0 - x)}{\Delta_w}\right)}{2}; & \Delta_0 - \Delta_w \leqslant x \leqslant \Delta_0 \end{cases} \tag{1}$$

where Φ_0 denotes the ratio of the monomer density and the value Φ in the middle of the film. The width Δ of an equivalent film with constant monomer density Φ is $\Delta = \Delta_0 - \Delta_w$. We choose $\Delta_w/R_e = 0.15 \ll 1$ [46] for computational convenience. If both polymer species are structurally symmetric, i.e., they are characterized by the same end-to-end distance, R_e, and their volumes are identical, they suffer the same entropy loss as they pack against the surface. Therefore, the surface free energy difference $\Delta\gamma$ is (largely) independent of the width of the boundary region Δ_w [47][2].

Both surfaces interact with the monomer species via a short-ranged potential H:

$$H(x) = \begin{cases} \dfrac{4\Lambda_1 R_e\left\{1+\cos\left(\frac{\pi x}{\Delta_w}\right)\right\}}{\Delta_w}; & 0 \leqslant x \leqslant \Delta_w \\ 0; & \Delta_w \leqslant x \leqslant \Delta_0 - \Delta_w \\ \dfrac{4\Lambda_2 R_e\left\{1+\cos\left(\frac{\pi(\Delta_0 - x)}{\Delta_w}\right)\right\}}{\Delta_w}; & \Delta_0 - \Delta_w \leqslant x \leqslant \Delta_0. \end{cases} \tag{2}$$

$H > 0$ is attractive for the A-monomers and repulsive for the B-species. The normalization of the surface fields Λ_1 and Λ_2, which act on the monomers close to the left and the right surface, is chosen such that the integrated interaction energy between the surface and the monomers is independent of the width of the boundary region Δ_w. As we shall see below, this condition makes the wetting transition temperature of a symmetric polymer mixture rather independent of Δ_w, but the length of the pre-wetting line (or the strength of the transition) depends on the width Δ_w of the surface boundary.

A- and B-polymers contain N monomers and are structurally symmetric. The polymer conformations $\{\mathbf{r}_\alpha(\tau)\}$ determine the microscopic A-monomer density $\hat{\Phi}_A(\mathbf{r}) = \frac{N}{\Phi}\sum_{\alpha=0}^{n_A}\int_0^1 d\tau\,\delta(\mathbf{r}-\mathbf{r}_\alpha(\tau))$, where the sum runs over all n_A polymers of type A in the system and $0 \leqslant \tau \leqslant 1$ parameterizes the contour of the Gaussian polymer. A similar expression holds for $\hat{\Phi}_B(\mathbf{r})$. With this definition the semi-grandcanonical partition function takes the form [12, 13]

$$\begin{aligned} \mathcal{Z} \sim \sum_{n_A=1}^{n} & \frac{e^{+\Delta\mu n_A/2k_BT}}{n_A!}\frac{e^{-\Delta\mu n_B/2k_BT}}{n_B!} \\ & \times \int\prod_{i_A=1}^{n_A}\mathcal{D}_{i_A}[\mathbf{r}]\mathcal{P}_A[\mathbf{r}]\int\prod_{i_B=1}^{n_B}\mathcal{D}_{i_B}[\mathbf{r}]\mathcal{P}_B[\mathbf{r}]\delta\left(\Phi_0 - \hat{\Phi}_A - \hat{\Phi}_B\right) \\ & \times \exp\left(-\Phi\int d^3\mathbf{r}\left\{\chi\hat{\Phi}_A\hat{\Phi}_B - H(\hat{\Phi}_A - \hat{\Phi}_B)\right\}\right) \end{aligned} \tag{3}$$

where $n = n_A + n_B$ and $\Delta\mu$ represents the exchange potential between A- and B-polymers. The functional integral $\mathcal{D}$ sums over all conformations of the Gaussian polymers with the

[2] In the presence of structural asymmetries in the segmental volumes, the loss of conformational entropy of the chains as they pack to comply with the density profile leads to an entropic contribution to $\Delta\gamma$. The effect can be estimated by the Lifshitz entropy formula (see [47])

statistical weight

$$\mathcal{P}[\mathbf{r}] \sim \exp\left(-\frac{3}{2R_{\mathrm{e}}^2}\int_0^1 \mathrm{d}\tau\,\left(\frac{\mathrm{d}\mathbf{r}}{\mathrm{d}\tau}\right)^2\right) \tag{4}$$

of a non-interacting Gaussian polymer (Wiener measure) [48]. The second factor enforces the monomer density profile to comply with equation (1) (incompressibility). The Boltzmann factor in the partition function incorporates the thermal repulsion between unlike monomers, which is described by the Flory–Huggins parameter χ, and the interactions between monomers and surfaces.

In the SCF theory, one introduces auxiliary fields Φ_{A}, ϕ_{B}, W_{A}, W_{B}, and Ξ to rewrite the partition function of the interacting multi-chain systems in terms of non-interacting chains in fluctuating fields. In the mean field approximation the free energy is obtained as the extremum of the semi-grandcanonical free energy functional $\mathcal{G}[\Phi_{\mathrm{A}}, \phi_{\mathrm{B}}, W_{\mathrm{A}}, W_{\mathrm{B}}, \Xi]$

$$\begin{aligned}\frac{\mathcal{G}}{nk_{\mathrm{B}}T} \equiv &+\ln\frac{n}{V_0} - \ln\mathcal{Q} + \frac{1}{V}\int \mathrm{d}^3\mathbf{r}\,(\chi N\Phi_{\mathrm{A}}\Phi_{\mathrm{B}} - HN\{\Phi_{\mathrm{A}} - \Phi_{\mathrm{B}}\})\\ &- \frac{1}{V}\int \mathrm{d}^3\mathbf{r}\,(\{W_{\mathrm{A}}\Phi_{\mathrm{A}} + W_{\mathrm{B}}\Phi_{\mathrm{B}}\} + \Xi\{\Phi_0 - \Phi_{\mathrm{A}} - \Phi_{\mathrm{B}}\})\end{aligned} \tag{5}$$

with respect to its arguments W_{A}, W_{B}, Φ_{A}, Φ_{B}, Ξ. $\mathcal{Q}_{\mathrm{A}}$ denotes the single chain partition function:

$$\mathcal{Q}_{\mathrm{A}}[W_{\mathrm{A}}] = \frac{1}{V_0}\int \mathcal{D}_1[\mathbf{r}]\mathcal{P}_{\mathrm{A}}[\mathbf{r}]\,\mathrm{e}^{-\int_0^1 \mathrm{d}\tau\, W_{\mathrm{A}}(\mathbf{r}(\tau))} \tag{6}$$

and similarly for $\mathcal{Q}_{\mathrm{B}}$, and $\mathcal{Q} = \exp(\Delta\mu/2k_{\mathrm{B}}T)\mathcal{Q}_{\mathrm{A}} + \exp(-\Delta\mu/2k_{\mathrm{B}}T)\mathcal{Q}_{\mathrm{B}}$.

The values of W_{A}, W_{B}, Φ_{A}, Φ_{B}, Ξ which extremize the free energy functional are denoted by lower-case letters and satisfy the self-consistent set of equations

$$w_{\mathrm{A}}(\mathbf{r}) = \chi N\phi_{\mathrm{B}}(\mathbf{r}) - H(\mathbf{r})N + \xi(\mathbf{r}) \tag{7}$$

$$\phi_{\mathrm{A}}(\mathbf{r}) = -\frac{V\mathrm{e}^{\Delta\mu/2k_{\mathrm{B}}T}}{\mathcal{Q}}\frac{\delta\mathcal{Q}_{\mathrm{A}}}{\delta w_{\mathrm{A}}(\mathbf{r})} \qquad \text{and} \tag{8}$$

$$\Phi_0(\mathbf{r}) = \phi_{\mathrm{A}}(\mathbf{r}) + \phi_{\mathrm{B}}(\mathbf{r}) \tag{9}$$

and similar expressions for w_{B} and ϕ_{B}. Substituting the extremal values of the densities and fields into the free energy functional (5) we calculate the free energy G of the different phases. At coexistence the two phases have equal semi-grandcanonical potential $\mathcal{G}$ at given χN and $\Delta\mu$.

To calculate the monomer density we employ the end segment distribution which satisfies a diffusion equation [43, 44]. We expand the spatial dependence of the densities and fields in a set of orthonormal functions [45, 46]. This procedure results in a set of non-linear equations which are solved by a Newton–Broydon method. We use up to 120 basis functions and achieve a relative accuracy 10^{-4} in the free energy in one-dimensional calculations.

We emphasize that there is no other approximation involved than the mean field approximation. In particular, we do not assume slowly spatial variation of the density profiles [49–51]. This condition is not fulfilled in the vicinity of the surfaces if $\Delta_{\mathrm{w}}/R_{\mathrm{e}} \ll 1$. The large and rapid density variation at the surface gives rise to pronounced local effects, e.g., deformation of the chain extension perpendicular to the surface or enrichment of chain ends. These result in corrections to the square gradient approximation [52–54]. The SCF calculations properly account for these phenomena on length scales down to a fraction of the coil extension. Non-universal packing effects on the length scale of a monomer are, of course, not incorporated in the Gaussian chain model. To this end, one has to replace the zero-ranged

interactions by a density functional and also consider the detailed molecular architecture on the short length scales via a partial enumeration scheme [40–42].

The SCF calculations have been extended to study the fluctuations and kinetics of phase separation [55–57]. In this case, one uses the free energy of the SCF theory as a function of the composition, $\phi_A(\mathbf{r})$, or the external field, $w_A(\mathbf{r}) - w_B(\mathbf{r})$, which is thermodynamically conjugated to the composition, to construct a purely relaxational dynamics that corresponds to class B in the scheme of Hohenberg and Halperin [58]. The underlying dynamics of the extended polymer molecules enters the description via the Onsager coefficient, which relates the gradient of the derivative of the free energy with respect to the dynamic variable to the current of that variable. If one uses the composition as a dynamic variable, different non-local expressions for the Onsager coefficient that are appropriate for Rouse-like and reptation-like dynamics are available [59]. Interestingly, if one uses the external potential as a dynamic variable (external potential dynamics [60]), a local Onsager coefficient corresponds to Rouse-like dynamics. The influence of the single molecule dynamics on the kinetics of collective concentration fluctuations has been investigated during the early stages of spinodal decomposition [56] in the bulk and the formation of enrichment layers at surfaces [55]. In both cases a local Onsager coefficient together with the external potential rather than the composition as a dynamic variable results in a much better agreement with simulation data and it is also computationally advantageous.

In the strong segregation limit $\chi_c^{\text{bulk}} N = 2 \ll \chi N \ll N$ many results of the SCF calculations are describable by simple analytic expressions. We shall denote these formulae by SSL in the following. For instance, the AB interface tension takes the form [61]:

$$\frac{\gamma_{AB} R_e^2}{k_B T} = \sqrt{\bar{N}}\sqrt{\chi N/6}\left(1 - \frac{4\ln 2}{\chi N} + \cdots\right) \qquad \text{(SSL)} \tag{10}$$

where $\bar{N} \equiv (\Phi R_e^3/N)^2$ is the invariant degree of polymerization.

The excess free energy of a surface in contact with the A-rich phase has two contributions. On the one hand the polymer conformations are restricted due to the presence of the surface. Since A- and B-polymers are assumed to have identical architectures, they lose the same conformational entropy as they pack against the surface. Hence, the difference in surface free energy between the two components is dominated by the surface energy. If the surface is completely covered by the A-component the surface energy per unit area amounts to $e_{\text{wall}}/k_B T = \Phi R_e \Lambda$ [46]. The surface energy density of a surface covered with B has the opposite sign. The experimentally relevant quantity is the strength of the monomer–surface interaction $\Lambda R_e \sim \Lambda\sqrt{N}$. In general, the interaction between the chemical constituents of the mixture and the surface does not depend on the molecular weight, and $\Lambda R_e \sim \Lambda\sqrt{N}$ is independent of the chain length N.

3. Wetting transition

To accurately locate the wetting transition and calculate the contact angle of macroscopic A-drops we use Young's equation [62]: $\gamma_{AB}\cos\Theta = \gamma_{WB} - \gamma_{WA} \equiv \Delta\gamma$. The results for our model are presented in figure 3. From the crossing of $\gamma_{AB}(\epsilon)$ and $\Delta\gamma(\epsilon)$ we accurately locate the wetting transition. The fact that curves intersect under a finite angle indicates that the wetting transitions are of first order. As we reduce the monomer–surface attraction the wetting transition shifts to higher temperatures $k_B T/\epsilon$ and becomes weaker. For all transitions studied, however, the wetting transition is of first order. This is also corroborated by SCF calculations [13, 63], where we find first order wetting transitions for $T/T_c < 0.98$.

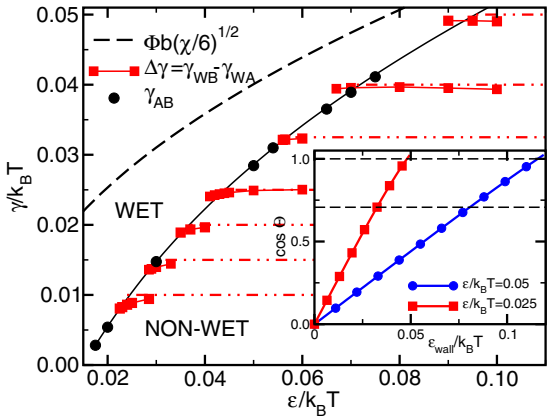

Figure 3. Interface tension γ_{AB} and difference in surface tensions $\Delta\gamma = \gamma_{WB} - \gamma_{WA}$ as a function of inverse temperature ϵ/k_BT obtained from simulations. Approximations for the interface tension $\gamma_{AB} = b\Phi\sqrt{\chi/6}$ in the strong segregation limit and $\Delta\gamma = 2\Phi d_{wall}\epsilon_{wall} = \epsilon_{wall}/4$ (dashed–dotted lines) are also shown. From [14]. The inset shows the dependence of the contact angle on ϵ_{wall} for the two temperatures investigated in section 5.

Computationally, Young's equation has distinct advantages for locating first order wetting transitions [14, 40]:

(i) The interface free energy γ_{AB} and the difference $\Delta\gamma = \gamma_{WB} - \gamma_{WA}$ can be measured accurately in separate simulations, thereby avoiding the need for huge simulation cells to simulate a thick A-layer at the surface in equilibrium with a B-rich bulk.

(ii) By virtue of the A $\leftrightharpoons$ B symmetry, the difference $\Delta\gamma$ can also be rewritten as the difference $\Delta\gamma = \gamma_{WB} - \gamma_{-WB}$ of surface tensions of a surface that attracts the A-component and a surface that attracts the B-component. This free energy difference can be measured by thermodynamic integration or expanded ensemble methods [14]. This method works best for wetting transitions that are strongly first order.

(iii) Unlike observing the dependence of the thickness of the A-layer on temperature or monomer–surface attraction, one directly measures free energies. Therefore, we do accurately locate the first order transition, while the instability of the A-rich layer is located somewhere between the transition and the mean field wetting spinodal. Moreover, determining the order of the transition from the observation (or absence) of metastability is not always easy.

In case of a first order wetting transition, there is a concomitant pre-wetting transition (see section 4.1). Locating the pre-wetting transition involves only enrichment layers of finite thickness (accessible to simulations of finite system sizes), and by extrapolating these data back to the coexistence curve we also obtain an accurate estimate. The metastability of enrichment layers or the apparent contact angle of microscopic drops is much less reliable [64, 41].

If the wetting transition is of first order, then there will be only a (vanishingly) small A-rich layer in the non-wet state. The surface free energy difference $\Delta\gamma$ is mainly enthalpic. If we assume that the wetting transition is strongly first order, we can neglect the microscopic enrichment layer at the surface and obtain $\Delta\gamma = 2\epsilon_{wall}d_{wall}\Phi$, where $d_{wall} = 2$ denotes the range of the monomer–surface interaction and $\Phi = 1/16$ the monomer number density. Using the expression for the interface tension $\gamma_{AB} = \Phi b\sqrt{\chi/6}$ (with $b \equiv R_e/\sqrt{N-1} = 3.05u$

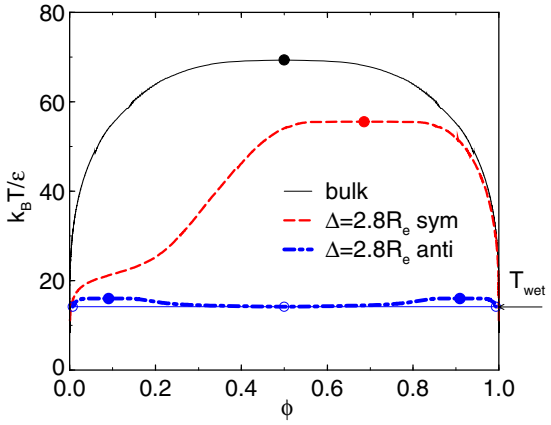

Figure 4. Phase diagrams in terms of composition and temperature for film width $\Delta \approx 2.8R_e$ as obtained from simulations. The arrow marks the wetting transition temperature. $\epsilon_{wall} = 0.16k_BT$. From [15].

being the statistical segment length) in the strong segregation limit [61], we obtain

$$\chi_{wet} = 24\left(\frac{\epsilon_{wall} d_{wall}}{bk_BT}\right)^2 \tag{11}$$

or, equivalently, in terms of the surface fields used in the SCF calculations, $\Lambda_{wet}N \approx \sqrt{\chi_{wet}N/24}(1 - \frac{4\ln 2}{\chi N} + \cdots)$.

This behaviour is in marked contrast to the value of the critical Flory–Huggins parameter at the unmixing transition in the bulk, $\chi_c = 2/N \sim 1/T_c \ll \chi_{wet}$ [14]. As both the interface tension γ_{AB} and the difference in surface tension $\Delta\gamma$ are chain length independent, so is the wetting transition temperature. The critical temperature T_c of phase separation, however, increases linearly with chain length N. Therefore, critical phenomena associated with the bulk unmixing and wetting phenomena are well separated (i.e., using the expressions for the strong segregation limit is justified), and polymer mixtures are good candidates for studying first order wetting transitions.

4. Thin films

4.1. Capillary condensation and interface localization/delocalization

If the mixture is confined into a film, the surface interactions modify the phase behaviour. As wetting is associated with the growth of an infinitely large enrichment layer, it is rounded-off in a thin film [5]. If the wetting transition is of first order, there will be a pre-wetting transition [1, 2]: a coexistence between a thin and a thick (but microscopic) enrichment layer at a chemical potential which differs from the value at coexistence in the bulk. As pre-wetting transitions involve only enrichment layers of finite thickness, they might give rise to transitions in thin films.

First, we regard a film with symmetric surfaces [14, 16], i.e., both surfaces attract the A-component. The phase diagram as obtained from the simulations is presented in figure 4. Compared to the phase behaviour in the bulk, the critical point is shifted to lower temperatures and larger composition of the species attracted by the surfaces [5]. The binodal in the vicinity of the critical points exhibits two-dimensional Ising (2DI) critical behaviour in contrast to the

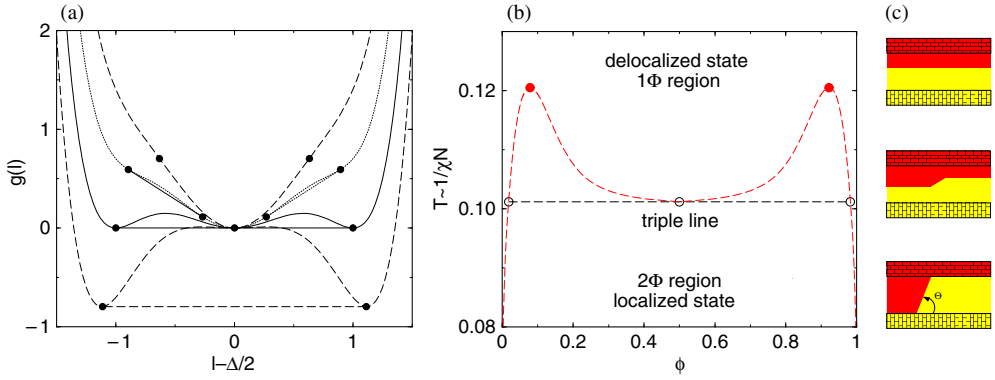

Figure 5. (a) Schematic temperature dependence of the effective interface potential in a film with antisymmetric surfaces. We assume that the wetting transition is of first order and that the film thickness is larger than the tricritical thickness (see the text for further explanation). This scheme does not correspond to simulation data or SCF calculations, but the lines are obtained by phenomenologically describing the interface potential by a sum of three exponentials (see [15] for explicit expressions). The temperatures correspond to $T < T_{\rm trip}$, $T_{\rm trip}$, $T_{\rm trip} < T < T_{\rm c}^{\rm film}$ and $T_{\rm c}^{\rm film}$. (b) Phase diagram of a mixture. (c) Sketches of typical configurations for $T > T_{\rm c}^{\rm film}$ (upper panel), $T_{\rm trip} < T < T_{\rm c}^{\rm film}$ in the miscibility gap (middle panel) and $T < T_{\rm trip}$ (lower panel) for $\langle\phi\rangle \neq 1/2$. From [16].

three-dimensional Ising (3DI) behaviour of the bulk unmixing transition. As we increase the film width Δ, the critical temperature gradually approaches the bulk critical temperature and the binodals of the film converge towards the bulk coexistence values.

We note, however, that this does not hold true for spinodal curves inside the miscibility gap, because phase separation in the film proceeds via the instability of AB interfaces that run parallel to the film surfaces (via interface fluctuations) rather than bulk-like composition fluctuations. Therefore, the spinodals in a film do not converge towards their bulk counterparts as $\Delta \to \infty$ [65].

Note the pronounced distortion of the B-rich binodal in the vicinity of the wetting transition. In the B-rich phase there are A-rich layers at the surfaces, and the B-component prevails in the middle of the film. In the vicinity of the wetting transition the thickness of the A-enrichment layers grows as we increase the temperature. If we increased the film thickness this distortion would evolve into an additional two-phase region [14, 66], corresponding to a B-rich phase with thin and thick A-layers at the surface. This two-phase region would correspond to the pre-wetting coexistence and it would join the B-rich binodal in a triple point.

The phase diagram of an antisymmetric film is also presented in figure 4. In this case one surface attracts the A-component with exactly the same strength as the other surface attracts the B-component. The phase diagram contains two critical points and a triple line [12, 13, 15]. Around the critical temperature of the bulk, enrichment layers gradually form at the surfaces and stabilize an AB interface that runs parallel to the surfaces. At the interface localization/delocalization transition [67–69] this AB interface becomes bound to one of the surfaces. In the case of a first order interface localization/delocalization transition this corresponds to a triple point of the phase diagram: an A-rich phase, a B-rich phase and a phase with symmetric composition coexist.

The behaviour can be analysed qualitatively by looking at the interface potential $g(l)$ which describes the interaction between an AB interface and a single surface. If the film is wide enough, the interface potential can be constructed as a superposition of the interface potentials emerging from each surface. The qualitative behaviour in the vicinity of a first

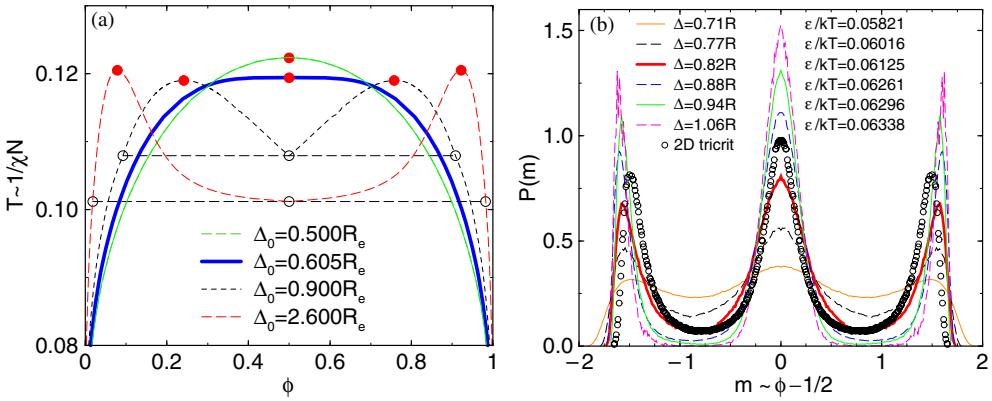

Figure 6. (a) SCF calculations for the dependence of the phase diagram on the film thickness Δ_0. For very thin films, the interface localization/delocalization transition is of second order even though the wetting transition is of first order. For $\Delta_{0\mathrm{tri}} = 0.605R_\mathrm{e}$ the transition is tricritical. In this case the binodals mirror the small exponent $\beta_\mathrm{tri}^\mathrm{MF} = 1/4$ of the tricritical mean field universality class. For all larger film thicknesses it is of first order. From [13]. (b) Probability distribution for various film widths as indicated in the key scaled to unit norm and variance. The incompatibility has been adjusted such that the peak heights correspond to the scaled universal distribution of the two-dimensional tricritical universality class. The latter distribution is shown as circles [71]. The lateral system size is $L = 5.6R_\mathrm{e}$. From [15].

order wetting transition is depicted in figure 5(a). Using a double-tangent construction we can obtain the phase behaviour in a thin film. At low temperatures there coexist an A-rich phase and a B-rich phase, in which the AB interface is localized at the surface. Upon increasing the temperature, one encounters the triple point. This triple point is the thin film analogy of the first order wetting transition. As the film width increases, the triple temperature converges towards the wetting transition temperature of the semi-infinite system. Above the triple temperature there are two phase coexistence regions, which correspond to thin and thick enrichment layers at the surfaces. This is the analogy of the pre-wetting transition in a thin film. If we increase the film width Δ, the miscibility gaps associated with the pre-wetting coexistence become narrower, $\delta\phi \sim 1/\Delta$. For each finite value of $\Delta < \infty$, the critical points are associated with the pre-wetting behaviour and not bulk criticality.

4.2. The tricritical interface localization/delocalization transition

If we reduce the film width, the interactions emerging from each surface interfere. Landau theory calculations [70] explain that this leads to a second order interface localization/delocalization transition at small film widths (with a single critical point). For large film thickness the transition is of first order. Both regimes are separated by a tricritical transition [70]. The dependence of the phase diagram on the film thickness as obtained from SCF theory is presented in figure 6(a). Estimating the tricritical film thickness from the MC simulations is computationally demanding. The scaled distribution functions prove convenient for accurately locating the tricritical width from the simulation data. To this end we have adjusted the temperature such that the central peak of the probability distribution of the order parameter $m \sim \phi_\mathrm{A} - \phi_\mathrm{B}$ is a factor 1.2 higher than the outer peaks. This corresponds to the behaviour of the universal distribution of the two-dimensional tricritical (2DT) universality class [71]. The results for various film widths Δ (in units of the lattice spacing) are presented in figure 6(b). For $\Delta < \Delta_\mathrm{tri}$ the valleys between the three peaks are too shallow (see figure 6),

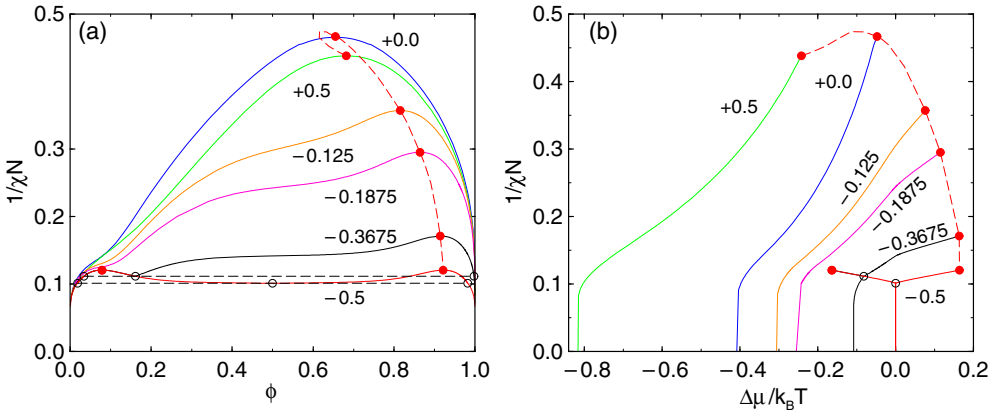

Figure 7. (a) Binodals for $\Delta_0 = 2.6R_e$ and surface interaction $\Lambda_1 N = 0.5$ obtained from SCF calculations. The surface interaction at the other surface $\Lambda_2 N$ varies as indicated in the key. The dashed curve shows the location of the critical points. Filled circles mark critical points, open circles/dashed horizontal lines denote three-phase coexistence for $\Lambda_2 N = -0.3675$ and -0.5. (b) Coexistence curves in the χN–$\Delta\mu$ plane. The 'quasi-pre-wetting' lines for $\Delta\mu < 0$ and $\Lambda_2 N = -0.3675$ and -0.5 are indistinguishable, because they are associated with the pre-wetting behaviour of the surface with interaction $\Lambda_1 N = +0.5$. From [12].

while they are too deep for $\Delta > \Delta_{tri}$. In the latter case the transition is of first order, and our estimate tends towards the triple temperature. At $\Delta_{tri} \approx 0.89R_e$ the distribution of our simulations is similar to the universal 2DT distribution, and this has been confirmed for larger lateral system sizes [15].

4.3. Crossover from capillary condensation to interface localization/delocalization

Realizing strictly (anti)symmetric surface interactions is often difficult in experiments. How does the phase behaviour vary between the two qualitatively different limits—capillary condensation and interface localization/delocalization—for not strictly symmetric or antisymmetric systems? By altering the surface interaction $\Lambda_2 N$ of the top surface from attracting the A-component to attracting the B-component (while the bottom surface always attracts the A-component with fixed strength $\Lambda_1 N$) in the SCF calculations, we study the crossover from capillary condensation for symmetric surfaces to interface localization/delocalization. The dependence of the phase diagram on the surface interactions within the SCF calculations is presented in figure 7. For symmetric surfaces (capillary condensation) the critical point is shifted towards lower temperatures [5], similar to the simulation result. The coexisting phases have almost uniform composition across the film and differ in their average composition. As we reduce the preference of the top surface for species B, the critical point and the critical composition tend towards their bulk values ($\phi = 0.5$, $1/\chi N = 0.5$), i.e., the critical temperature increases and the critical composition becomes more symmetric [12]. The coexistence curve in the $1/\chi N$–$\Delta\mu$ plane approaches the symmetry axis. Upon making the top surface attracting the other component, B, we gradually change the character of the phase transition towards an interface localization/delocalization transition [67, 68]. The critical temperature passes through a maximum and the critical composition through a minimum, respectively. For $\Lambda_2 N < 0$ (surface attracting the B-component) there are enrichment layers of the A-component at the bottom and the B-component at the top, and the two coexisting phases differ in the location of the AB interface which runs

parallel to the surfaces. As the preferential interaction of the top surface increases, the critical temperature decreases and the critical composition becomes richer in A. When the coexistence curve intersects the pre-wetting line of the bottom surface at $\Delta\mu < 0$, a triple point forms at which an A-rich phase and two B-rich phases with a thin and a thick A-enrichment layer coexist. When the bottom surface attracts the component A with exactly the same strength as the top surface the component B (antisymmetric surfaces), the phase diagram becomes symmetric.

4.4. Length scale of the interface potential $g(l)$

The effective interface potential $g(l)$ is a key to describing the wetting behaviour. Within mean field theory, much of the influence of the wetting behaviour on the phase transitions in thin films can be understood from the interface potential (see section 4.1).

Both in our MC simulations as well as in our SCF calculations the monomer–surface interactions are strictly short ranged, while in experiments the van der Waals interactions between the constituents of the surface and the polymer fluid will also give rise to an additional long-ranged contribution to the interaction. We note that the qualitative interplay between wetting and phase separation in thin films will remain unaltered as long as the wetting transition is of first order. Of course, this qualitative similarity does not hold true for power laws that describe the growth of the wetting layer at a second order wetting transition or complete wetting, and, in particular, fluctuation effects depend strongly on the range of the interface potential.

In the case of short-ranged forces, the interaction between the AB interface and the surfaces stems from a distortion of the composition profile in the vicinity of the surface. The interaction decays exponentially with the distance l between the interface and the surface, and the length scale of the decay $1/\lambda$ is set by the characteristic length scale of the interface profile. In a binary polymer blend, however, the intrinsic profile (i.e., without considering capillary waves) of the interface between the two coexisting phases in the bulk is characterized by two length scales: the width $w_{\mathrm{SSL}}/2$ characterizes the slope of the profile at the centre. In the strong segregation limit, $\chi N \gg 2$, it is independent of the chain length and decreases with increasing incompatibility: $w_{\mathrm{SSL}} = R_{\mathrm{e}}/\sqrt{6\chi N}$. This length scale is set by the size of polymer loops across the interface, which on average cost a free energy comparable to $k_{\mathrm{B}}T$. Far away from the centre, the profile approaches the composition of the coexisting phases exponentially, and the characteristic length scale is set by the correlation length ξ of composition fluctuations of the bulk. The latter quantity becomes independent of the incompatibility and is of the order $R_{\mathrm{e}} \sim \sqrt{N}$ for $\chi N \gg 2$. In the weak segregation limit, $\chi N - 2 \sim \mathcal{O}(1)$, the two length scales become identical, $w \sim R_{\mathrm{e}}$. Which of the two length scales characterizes the decay of the interface potential $g(l)$ in binary polymer blends?

To this end, we have calculated the free energy density f of an antisymmetric film in the SCF theory as a function of the composition ϕ for various film widths and two temperatures, $\chi N = 5$ and 8. Those temperatures are above the critical temperature of the film, and the AB interface is localized in the middle of the film. Around $\phi = 1/2$ the free energy density can be expanded in the form $f = f_1 + f_2(\phi - 1/2)^2$. This yields for the effective AB interface potential $g(l) = \Phi k_{\mathrm{B}}T\Delta f/N \sim \text{constant} + f_2(l - \Delta/2)^2/\Delta$. Above the critical temperature we can estimate the effective range $1/\lambda$ of the interaction according to $g(l) \sim \exp(-\lambda\Delta/2) \sim f_2/\Delta$. In figure 8 we plot f_2/Δ versus the film width Δ. For large film widths the data exhibit an exponential dependence on the film width. Upon increasing the temperature the interaction increases as the surfaces repel the AB interface stronger. For small Δ, i.e., distances between the AB interface and the surface which are not very much larger than the interfacial width w,

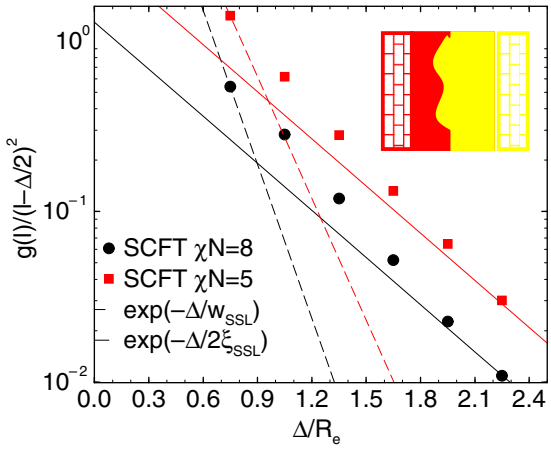

Figure 8. Curvature of the interface potential at the centre of the film. The symbols represent SCF calculations for $\chi N = 5$ and 8, and $\Lambda N = 0.5$. The solid lines correspond to $g \sim f_2/\Delta \sim \exp(-\lambda\Delta/2)$ with $1/\lambda = \xi$, while the dashed lines depict the behaviour for $1/\lambda = w_{\mathrm{SSL}}/2$.

the interaction decays somewhat faster, $w < 1/\lambda < \xi$. For large Δ the interaction range is compatible with $1/\lambda = \xi \approx R_{\mathrm{e}}/\sqrt{18}$, where we have used the behaviour of the correlation length at strong segregation.

4.5. Fluctuation effects

Fluctuation effects are important in the vicinity of critical points. Of course, the binodals are parabolic in mean field theory independent of dimensionality (see figure 7), while the MC simulations yield much flatter binodals in accord with the Ising universality class in three [30] and two dimensions (see figure 4). Simulation data for the bulk phase behaviour [32, 17] show that the mean field theory becomes quantitatively accurate in the limit $\bar{N} \to \infty$, as expected from the Ginzburg criterion [18].

In a symmetric polymer blend, however, wetting occurs far below the critical point; hence, critical, bulk-like fluctuations of the composition are not important for the wetting behaviour. The fluctuations of the local interface position, i.e., capillary waves are the pertinent fluctuations that may modify the mean field predictions on wetting [1, 2]. Instead of minimizing the free energy $g(l)$ of a (hypothetically) flat interface that interacts with the confining surfaces, the behaviour of the fluctuating AB interface, which is bound to the surface, can be described via an effective Hamiltonian. Many theoretical investigations have been directed towards the detailed form of this Hamiltonian [72, 73]. In its simplest, most basic form this Hamiltonian

$$\frac{\mathcal{H}_{\mathrm{eff}}[l]}{k_{\mathrm{B}}T} = \int \mathrm{d}x\,\mathrm{d}y\,\left\{\frac{\gamma}{2}(\nabla\delta l(x,y))^2 + \frac{1}{2}\frac{\partial^2 g}{\partial l^2}\delta l^2\right\} \tag{12}$$

comprises a contribution from the increase of the interface area due to deviations δl of the local interface position from its average value $\langle l\rangle$ and the effect of the interface potential $g(l)$. x and y denote the coordinates parallel to the interface.

4.5.1. Interface tension and its position dependence. The validity of the coarse-grained interface description by the Hamiltonian (12) can be assessed by computer simulations. The results (especially at small length scales) depend somewhat on which method is used to extract

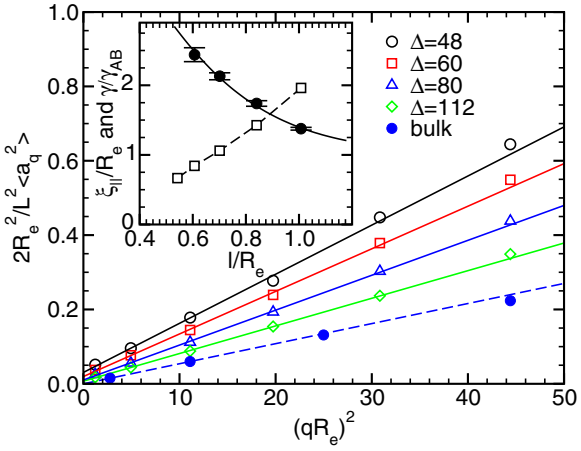

Figure 9. Fluctuation spectrum of the AB interface for different system sizes Δ. The solid lines corresponds to fits in the range $0 < (qR_e)^2 < 34.6$. The dashed line corresponds to capillary fluctuations with $\gamma_{AB} = 0.054$, the value measured independently via re-weighting techniques. The filled circles represent the capillary fluctuation spectrum in the bulk system ($3.8R_e \times 3.8R_e \times 7.5R_e$ geometry and periodic boundary conditions). The inset shows the ratio of the effective interface tension and its bulk value (circles) and the parallel correlation length $\xi_\parallel$ on the thickness l of the wetting layer. From [14].

$l(x, y)$ from the simulation snapshots. We use an integral criterion [74] for the local, y-averaged interface position:

$$l(x) = \frac{\int_0^{\Delta/2} \mathrm{d}z \int \mathrm{d}y\, \phi_A(x, y, z)}{\frac{2}{\Delta}(2\langle\phi\rangle - 1)\int_0^{\Delta/2} \mathrm{d}z \int \mathrm{d}y\, [\phi_A(x, y, z) + \phi_B(x, y, z)]} + \text{constant}. \tag{13}$$

The local interface position can be Fourier decomposed according to

$$l(x) \sim \frac{a_0}{2} + \sum_{k=0}^{L/2-1} \left[a_{q_k} \cos(q_k x) + b_{q_k} \sin(q_k x)\right] \tag{14}$$

with $q_k = 2\pi k/L$. Using the equipartition theorem, we find that the Fourier amplitudes are Gaussian distributed and their variances are given by

$$\frac{2}{L^2\langle a_q^2\rangle} = \frac{\gamma}{k_B T}\left\{q^2 + \frac{\mathrm{d}^2 g}{\gamma\, \mathrm{d}l^2}\right\} = \frac{\gamma}{k_B T}\left\{q^2 + \left(\frac{2\pi}{\xi_\parallel}\right)^2\right\} \tag{15}$$

where we have used a quadratic expansion of the interface potential around its average, equilibrium position. The interaction between the interface and the surfaces, $g(l)$, imparts a parallel correlation length $\xi_\parallel$ onto the interface fluctuations which cuts off the spectrum at large length scales.

Simulations of unconfined interfaces [33, 75] have shown that the Fourier amplitudes are indeed Gaussian distributed and that γ can be identified with the interface tension γ_{AB}, which has been measured independently. This is illustrated by the full circles in figure 9 that display the spectrum of interface fluctuations of an unconfined interface (using a local criterion for the interface position [33]), whereas the dashed curve corresponds to the prediction (15) with $g = 0$ and $\gamma = \gamma_{AB}$ as determined independently via a re-weighting technique. The effective interface Hamiltonian yields an accurate description of the fluctuations of a non-interacting interface on large length scales. By analysing larger wavevectors we can extract higher order terms that correspond to the bending rigidity of the interface [33, 40].

The other data in figure 9 refer to a confined system with symmetric boundary conditions at capillary condensation (in the B-rich phase). The open symbols denote simulation results, whereas the solid lines present linear regressions according to equation (15). The fit yields the parallel correlation length $\xi_\parallel$ and the effective interface tension γ, and the results are presented in the inset of figure 9. To extract the parallel correlation length we have assumed that the interface tension γ in the interface Hamiltonian corresponds to the value of an unbound interface, γ_{AB}. Unfortunately, the integral definition of the local interface position is affected by bulk composition fluctuations, which result in an overestimation of the fluctuations of the local interface position. However, assuming that these bulk composition fluctuations are laterally uncorrelated on length scales $2\pi/q$ larger than the bulk correlation length ξ, we can take them into account by the substitution

$$\left(\frac{\mathrm{d}^2 g}{\mathrm{d}l^2}\right)^{-1}_{\mathrm{eff}} \approx \left(\frac{\mathrm{d}^2 g}{\mathrm{d}l^2}\right)^{-1} + \frac{\Delta\chi_+}{2(2\langle\phi\rangle - 1)^2} \tag{16}$$

where χ_+ is the susceptibility of the A-rich phase. Thus, bulk composition fluctuations mainly influence our estimate of $\xi_\parallel$. However, we can still use equation (15) to extract an effective interface tension γ for $0 < q < 2\pi/\xi$. The results for γ as a function of the distance l are presented in the inset of figure 9. Most notably, the effective interface tension, γ, for width $\Delta = 2.8R_e$ is more than twice as large as γ_{AB} of a free interface. For a larger distance between the interface and the surface, γ approaches the interface tension of the free AB interface, γ_{AB}.

4.5.2. Renormalization of $g(l)$ by capillary waves. In the SCF calculations the range of the interface potential is set by the correlation length ξ of the bulk composition fluctuations. Fluctuations of the local interface position—i.e., capillary waves—give rise to corrections to the mean field theory. The renormalization of $g(l)$ by fluctuations has attracted longstanding interest [72, 73, 76, 77]. Qualitatively, capillary waves cause the interface to fluctuate locally around the minimum of the interface potential and to average over a small region around the minimum. If the interface tension γ_{AB} is large, the fluctuations are suppressed and the renormalization is small; if the interface tension is small, the interface makes rather large excursions around the preferred position and fluctuation effects are important. The strength of the fluctuation effects can be characterized by the dimensionless capillary parameter ω:

$$\omega = \frac{k_B T}{4\pi\gamma_{AB}\xi^2} = \begin{cases} \omega_{3DI} \approx 0.86 & \chi N - \chi_c N \ll 1/\bar{N} \quad \text{Ising critical regime} \\ \dfrac{(2\chi N - 2)^{-1/2}}{\sqrt{\bar{N}}} & 1/\bar{N} \ll \chi N - 2 \ll 1 \quad \text{weak segregation} \\ \dfrac{9}{2\pi\sqrt{\bar{N}}\sqrt{\chi N/6}} & 1 \ll \chi N - 2 \quad \text{strong segregation.} \end{cases} \tag{17}$$

In the ultimate vicinity of the critical point, polymer mixtures exhibit Ising critical behaviour and the capillary parameter adopts a universal, constant value. At lower temperatures, however, ω becomes small both upon increasing χN and the invariant degree of polymerization $\bar{N} \equiv (\Phi R_e^3/N)^2$. Note that the latter parameter does not influence the mean field prediction for the phase behaviour or wetting. Hence, by increasing $\bar{N}$ we can reduce the effect of fluctuations (both critical composition fluctuations in the vicinity of the critical point as well as capillary waves) without altering the phase behaviour or other predictions of mean field theory. In the limit $\bar{N} \to \infty$ the fluctuation effects become vanishingly small, while for short chain length one observes fluctuations similar to mixtures of simple molecules.

In figure 10 we determine the decay length of the interface potential from a MC simulation of a film with symmetric boundaries above the wetting transition temperature, $T \approx 3.55T_{wet}$

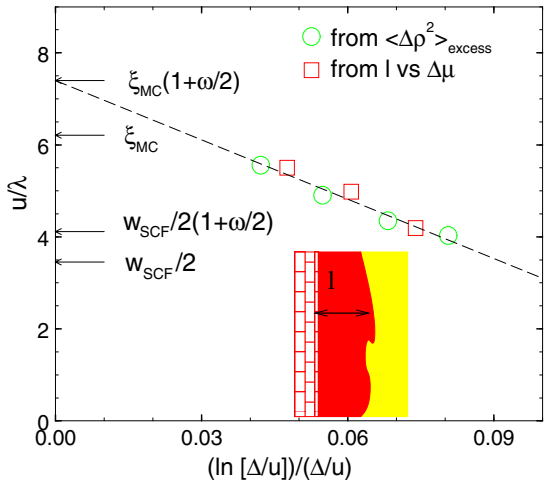

Figure 10. Measurement of the effective range $1/\lambda$ of the interaction between the surface and an interface in a thin film with symmetric boundary conditions. All lengths are given in units of the lattice constant $u = 0.059R_e$. The circles correspond to an estimate via the excess composition fluctuations in the MC simulations while the squares correspond to a measurement according to equation (18). The temperature $k_BT/\epsilon = 50$ is above the wetting temperature $k_BT/\epsilon_{wet} = 14.1(7)$. The arrows on the left-hand side denote possible candidates: the intrinsic width w of the AB interface, the bulk correlation length ξ and the renormalized values. From [14].

(complete wetting). The range of the potential $1/\lambda$ (squares) can be extracted from the dependence of the thickness of the enrichment layers on the exchange potential $\Delta\mu$ above the wetting transition temperature:

$$\langle l\rangle = \frac{1}{\lambda}\ln\frac{NA\lambda}{-\Phi(2\langle\phi\rangle - 1)\Delta\mu} \tag{18}$$

where A parameterizes the strength of the interface potential $g(l) = A\exp(-\lambda l)$. The slope $-\mathrm{d}\langle l\rangle/\mathrm{d}\ln\Delta\mu = 1/\lambda$ is displayed in the figure. The simulation data were obtained at coexistence. The value of the chemical potential $\Delta\mu_{coex}$ depends on the film width via Kelvin's equation, $\Delta\mu_{coex} \sim 1/\Delta$.

Alternatively, the capillary waves of the interface give rise to excess fluctuations of the composition.

$$\langle\Delta\phi^2\rangle_{excess} = \frac{\chi_- - \chi_+}{L^2\Delta} = \frac{2}{\Delta^2}(2\langle\phi\rangle - 1)^2\langle\delta l^2\rangle \tag{19}$$

where $\chi_\pm$ are the susceptibilities in the A-rich and A-poor phases, respectively. Using $L^2\langle\delta l^2\rangle = \left(\frac{\mathrm{d}^2 g}{\mathrm{d}l^2}\right)^{-1}$ and equation (18), we can estimate the interaction range $1/\lambda$ in a single simulation via

$$\frac{1}{\lambda} = \frac{\Phi}{2N(2\langle\phi\rangle - 1)}(\Delta\mu_{coex})\Delta^2L^2\langle(\Delta\phi)^2\rangle_{excess}. \tag{20}$$

The results of this measurement (circles) agree well with the results from the adsorption isotherm (squares). The range is larger than the intrinsic width of the interface w_{SCF} obtained from SCF calculations. When we extrapolate the results to infinite film width $\Delta \to \infty$, the MC data are compatible with the theoretical prediction $1/\lambda = \xi(1 + \omega/2)$ [72] for $T > T_{wet}$.

Direct information on the effective interface potential $g(l)$ can be obtained from the probability distribution of the composition in the vicinity of the wetting transition temperature

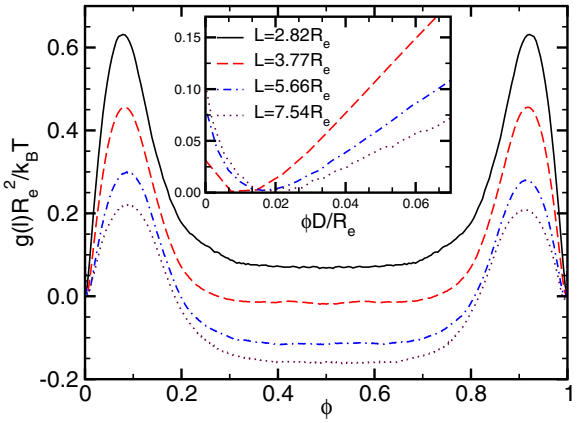

Figure 11. Dependence of the effective interface potential $g(l)$ on the lateral film extension L for $\Delta = 2.8R_e$ and $\epsilon/k_BT = 0.069$. The inset presents an enlarged view of the minimum of the localized state. From [15].

for an antisymmetric film. Since the wetting transition occurs in the strong segregation limit, the coexisting phases in the bulk are almost pure $\langle\phi\rangle \approx 0$ or 1, and bulk-like composition fluctuations can be neglected. Hence, the distance l between the surface and the interface is given by $l = \Delta\phi$, and the effective interface potential $g(l)$ can be measured in the MC simulations according to $g(l) = -k_BT/L^2 \ln P(\phi)$, where $P(\phi)$ denotes the probability distribution of the composition.

The result for the effective interface potential $g(l)$ in the vicinity of the triple point is presented in figure 11. The three minima correspond to the A-rich phase, the phase with the delocalized interface, and the B-rich phase. Unlike the situation at the tricritical point, the position of the minima does not depend on the lateral system size. Within mean field theory, the interface potential is independent of the lateral extension L. In the MC simulations, however, the effective interface potential does depend on L: the minima broaden upon increasing the lateral system size L and the free energy of the delocalized state decreases with respect to the localized ones. This dependence of $g(l)$ on the lateral system size gives rather direct evidence for a renormalization of the effective interface potential by interface fluctuations [78, 79] in the framework of a microscopic model.

The behaviour can be qualitatively rationalized as follows. Since the interface is constrained by the surfaces, the interface potential gives rise to a parallel correlation length, $\xi_\parallel \sim \sqrt{\mathrm{d}g^2/\mathrm{d}^2\phi}$ (see equation (15)), which acts as a cut-off for the spectrum of capillary waves. For lateral distances smaller than $\xi_\parallel$ the local position fluctuates like a free interface; for lateral distances that exceed $\xi_\parallel$ interface fluctuations are strongly suppressed [2]. From the curvature of $g(l)$ it is apparent that this parallel correlation length $\xi_\parallel$ is larger in the delocalized state than in the localized ones.

Interface fluctuations reduce the free energy of the system. Since more modes of interface fluctuations can be thermally excited in the delocalized state (larger $\xi_\parallel$) than in the localized one, the former can reduce its free energy with respect to the latter by interface fluctuations. This effect is important for accurately locating the triple temperature.

For the parameters of the simulation the lateral system size and the parallel correlation lengths are of the same order of magnitude. In the MC simulations the lateral system size L additionally cuts off interface fluctuations when $L < \xi_\parallel$ [74]. For very small L, the lateral system size determines the number of modes that can be excited in both states, and the relative

free energy difference does not depend on L. In an intermediate regime of lateral sizes $\xi_{\mathrm{loc}} < L < \xi_{\mathrm{deloc}}$ (shown in figure 11), the free energy of the localized state is independent of L, because ξ_{loc} acts as a cut-off for interface fluctuations, while we can reduce the free energy of the delocalized state by increasing L, because more and more (long wavelength) interface fluctuations build up. This effect can be observed in figure 11. For very large $L > \xi_{\mathrm{deloc}}$ (not accessible in the simulations), the spectrum of interface fluctuations also becomes independent of L for the delocalized state.

The effect of interface fluctuations is clearly observable in the MC simulations. In the previous section, we have focused on their influence on the interface potential. Additionally, they broaden the apparent interface profiles that are observed in simulations and experiments—a fact that has to be duly accounted for when comparing simulations/experiments to the prediction of the SCF theory [74]. Moreover, they can disorder highly swollen lamellar phases in mixtures of homopolymers and diblock copolymers into a microemulsion as observed in simulations [33], experiments [80], and more recently in SCF calculations [81] that include fluctuations.

5. Interface localization/delocalization in an antisymmetric double wedge

5.1. Background

In the following we consider wetting (or rather filling) in a wedge geometry. Macroscopic considerations show that the wedge will be filled with liquid when the contact angle Θ on a planar substrate equals the opening angle α. Intriguingly, Parry and co-workers [82] predict that the filling of a wedge is related to the strong fluctuation regime of critical wetting and that critical filling may even occur if the concomitant wetting transition of the planar surface is of first order. Specifically, they predicted the distance l_0 of the AB interface from the bottom of a wedge to diverge as $l_0 \sim (T_{\mathrm{f}} - T)^{-\beta_{\mathrm{s}}}$ with $\beta_{\mathrm{s}} = 1/4$. Correlations along the wedge and in the other two directions are characterized by diverging correlation lengths $\xi_y \sim (T_{\mathrm{f}} - T)^{-\nu_y}$ and $\xi_x \sim \xi_\perp \sim (T_{\mathrm{f}} - T)^{-\nu_\perp}$ with exponents $\nu_y = 3/4$ and $\nu_\perp = 1/4$, respectively, for short-ranged surfaces forces in three dimensions.

We study a wedge with opening angle $\alpha = \pi/4$ of the wedge (see figure 12). Similarly to the study of wetting, we use an antisymmetric geometry and stack two wedges which attract different components on top of each other. This antisymmetric double wedge is a pore with quadratic cross-section of size $L \times L$. Let L_y denote the length of the wedge (see figure 12). Such a geometry is advantageous:

(i) If we used identical surface fields on all four free surfaces the analogy of capillary condensation would occur in a wedge, i.e., phase coexistence would be shifted away from the bulk coexistence curve and the wetting layers would be only metastable (with respect to 'wedge condensation').
(ii) As wetting layers grew on all four surfaces in the case of symmetric boundaries, we would need larger system sizes to reduce the interactions between the wetting layers across the wedge.

The phase behaviour in such an antisymmetric double wedge geometry has been studied recently in the framework of an Ising model [22]. When the wetting transition of the planar substrate was of first order, the wedge filling was also found to be of first order. When the wetting transition was of second order, an unconventional scaling behaviour was observed which is characterized by critical exponents $\alpha = 3/4$, $\beta = 0$, and $\gamma = 5/4$. Those

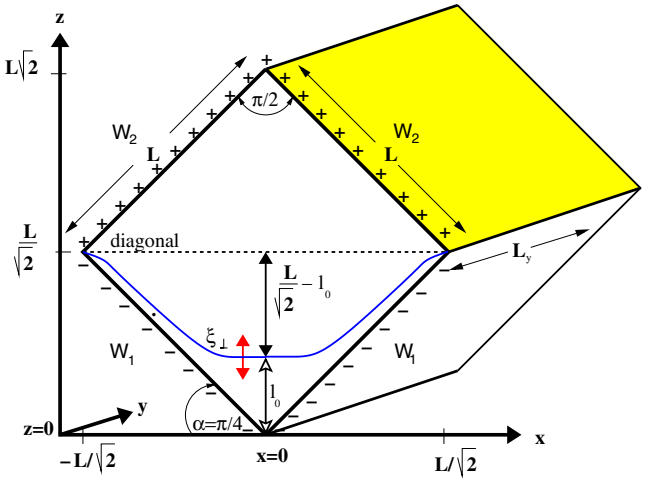

Figure 12. Antisymmetric double wedge: periodic boundary conditions apply along the y-direction and there are four impenetrable surfaces of size $L \times L_y$. The bottom ones (W_1) attract the A-component with strength ϵ_{wall} and the top ones (W_2) attract the B-component. l_0 denotes the position of the interface from one corner. From [22].

critical exponents can be related (see below) to the exponents of critical wedge filling, and the simulations of the Ising model confirm the predictions of Parry and co-workers [82].

In the following we corroborate these findings in the framework of the Ising model by our polymer simulations. Moreover, we present evidence for the unconventional second order transition in an antisymmetric double wedge even if the wetting transition on a planar substrate is of first order. This might be of practical relevance, because there exist no solid substrates that exhibit a second order wetting transition.

We present simulation data for two temperatures: $\epsilon/k_{\text{B}}T = 0.025$ ($T/T_{\text{c}}^{\text{bulk}} = 0.58$) and $\epsilon/k_{\text{B}}T = 0.05$ ($T/T_{\text{c}}^{\text{bulk}} = 0.29$). At both temperatures the wetting transitions, that occur at appropriate attractive strength ϵ_{wall} of planar surfaces, are of first order (see figure 3). In the former case it is a weak first order wetting transition; in the latter case it is a strong first order transition.

5.2. First order transition in an antisymmetric double wedge

At the lower temperature $\epsilon/k_{\text{B}}T = 0.05$, the behaviour is similar to a first order interface localization/delocalization transition. We consider here only the case $\Delta\mu = 0$ where phase coexistence in the bulk occurs. This excludes the rather interesting interplay between pre-wetting and pre-filling behaviour studied in [83]. At large surface interaction, $\epsilon_{\text{wall}} > \epsilon_{\text{wall}}^{\text{trip,wedge}}$, there runs an AB interface along the diagonal which divides the two double wedges (see figure 12). This corresponds to the delocalized state. Upon decreasing ϵ_{wall} (or decreasing the temperature) the AB interface becomes localized in one of the wedges. In this case the composition of the double wedge is either A-rich or B-rich and we define $m \equiv \phi_{\text{A}} - \phi_{\text{B}}$ as the order parameter. The two situations are separated by a triple point $\epsilon_{\text{wall}}^{\text{trip,wedge}}$ at which the interface can be localized in either of the wedges or be delocalized on the diagonal. The trimodal probability distribution in the vicinity of the tricritical point is presented in figure 13. In analogy to the case of antisymmetric films we expect this triple point in a double wedge to correspond to a first order filling transition. In the inset we show the cumulant $\langle m^2\rangle/\langle|m|\rangle^2$ as a function

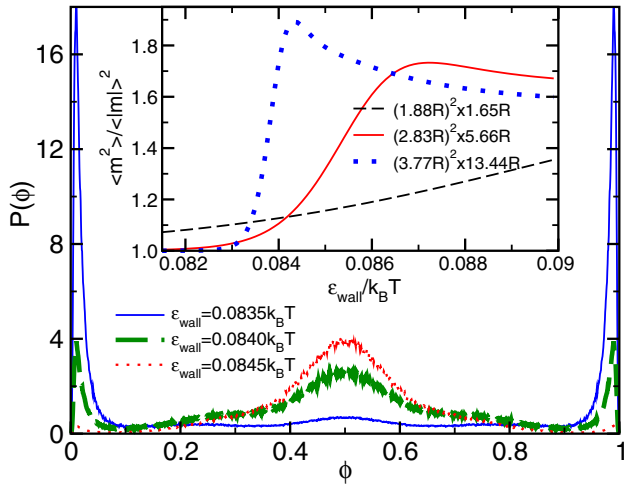

Figure 13. The probability distribution of the composition at $\epsilon/k_{\mathrm{B}}T = 0.05$ and system geometry $3.8R_{\mathrm{e}} \times 3.8R_{\mathrm{e}} \times 13.4R_{\mathrm{e}}$ exhibits a three-peak structure, which is characteristic of a first order transition. The inset shows the dependence of the cumulant $\langle m^2\rangle/\langle|m|\rangle^2$ with $m \sim \phi - 1/2$ on ϵ_{wall} for three different system sizes.

of the surface interaction strength ϵ_{wall}. If the transition was of second order, these cumulants would depend monotonically on ϵ_{wall} and would exhibit a common intersection point [84]. This is not at all what we observe, and we conclude that the interface localization/delocalization transition in the double wedge is of first order at the lower temperature $\epsilon/k_{\mathrm{B}}T = 0.05$.

5.3. Critical behaviour in an antisymmetric double wedge

Even though the wetting transition on a planar surface at $\epsilon/k_{\mathrm{B}}T = 0.025$ is of first order, the behaviour at the interface localization/delocalization transition in an antisymmetric double wedge at high temperature differs from the first order interface localization/delocalization transition at low temperature.

To locate the transition temperature, we use the macroscopic criterion for the contact angle $\cos\Theta = \Delta\gamma/\gamma_{\mathrm{AB}} = 1/\sqrt{2}$. Both the interface tension γ_{AB} and the difference in the surface tensions $\Delta\gamma = \gamma_{\mathrm{WB}} - \gamma_{\mathrm{WA}}$ can be accurately measured by re-weighting techniques (see section 3). The interface tension has been extracted from a simulation cell of size $L \times L \times 2L$ with periodic boundary conditions in all directions. The values of the interface tension do not strongly depend on the system size: the leading order finite size effects are only of the order $\ln L/L^2$. The difference $\Delta\gamma$ has been extracted from a symmetric film of width Δ. The leading order finite size effect of $\Delta\gamma$ is larger than the error in γ_{AB} and it scales like $1/\Delta$. This finite size effect arises from the finite compressibility and fluid structure of the polymer melt. In the vicinity of the surfaces, there are fluid-like packing effects that give rise to oscillations in the monomer density profile. On average, the density in the vicinity of the surface is slightly smaller than at the centre of the film or wedge. At constant total density $\Phi = (n_{\mathrm{A}} + n_{\mathrm{B}})N/(L^2\Delta)$ (as opposed to constant pressure), the density profile across the film takes the form $\Phi(z) \approx \Phi(1 + c/\Delta)\rho(z)$, where $\rho(z)$ denotes the normalized density profile and $c \approx \int \mathrm{d}z\ (1 - \rho(z)) > 0$. Due to the width dependence of the density, $\Delta\gamma$ also depends like $\epsilon_{\mathrm{wall}}(1 + c/\Delta)$ on the film width. Similar packing-induced effects have been observed previously in the measurement of the wetting transition temperature [14] and the dependence

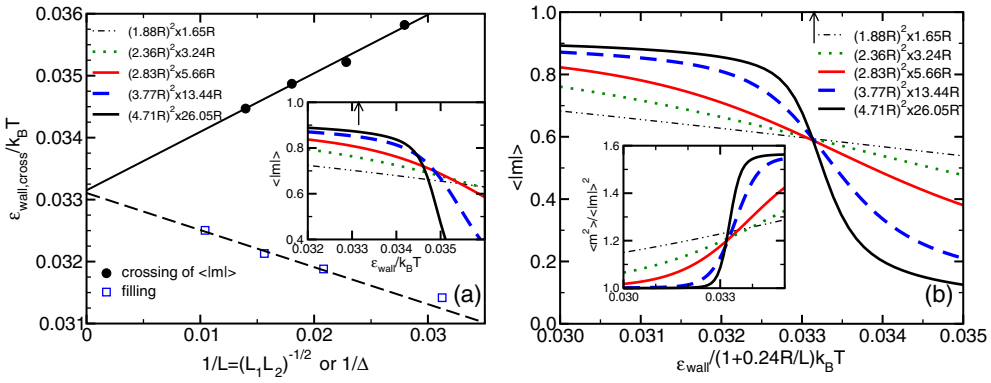

Figure 14. (a) Inset: dependence of the absolute value of the order parameter $m \equiv (\phi_A - \phi_B)$ on the surface interactions ϵ_{wall}/k_BT at the higher temperature $\epsilon/k_BT = 0.025$. Main panel: the values $\epsilon_{wall,cross}/k_BT$ (circles) at which the order parameter curves of two neighbouring systems sizes, L_1 and L_2, intersect are plotted against the inverse system size. The squares represent the location of the wedge filling transition as determined from the macroscopic condition $\cos\Theta = \Delta\gamma/\gamma_{AB} = 1/\sqrt{2}$. The system size dependence stems from $\Delta\gamma$, which has been extracted from a symmetric film of width Δ. The lines represent linear fits to accurately locate the transition of the infinite system at $\epsilon_{wall}/k_BT = 0.3315$. (b) Dependence of the absolute value of the order parameter $m \equiv |\phi_A - \phi_B|$ on the surface interactions $\epsilon_{wall}/(1+0.24R_e/L)k_BT$ at $\epsilon/k_BT = 0.025$. The inset shows the cumulant. From the crossing points we can accurately locate the localization/delocalization transition in the antisymmetric double wedge, $\epsilon_{wall}/k_BT = 0.3315$ of the infinite system.

of the critical temperature on the film width in antisymmetric films [15]. To account for this finite size effect we plot the data in figure 14(a) versus $1/\Delta$ and estimate the location of the filling transition at $\epsilon^{crit}_{wall}/k_BT = 0.3315$.

In the inset of figure 14(a) we present the dependence of the absolute value of the order parameter, $|m| \equiv |\phi_A - \phi_B|$, on the surface interaction strength for various system sizes. Curves that correspond to different system sizes cross in the vicinity of our estimate of the filling transition, but there is a systematic shift of the crossing point to smaller values of ϵ_{wall} upon increasing the lateral size L of the wedge. In the main panel, we plot the intersection points $\epsilon_{wall,cross}(L_1, L_2)$ of neighbouring system sizes L_1 and L_2 versus $1/\sqrt{L_1L_2}$. Again, the data fall onto a straight line and the data in the limit $L \to \infty$ are very well compatible with the estimate of the filling transition from the contact angle measurements in planar geometry.

In the following we account for these packing-induced effects by scaling the monomer–surface interaction ϵ_{wall} by a factor $1 + 0.24R_e/L$ chosen such that the absolute value of the magnetization exhibits a common intersection point as a function of $\epsilon'_{wall} \equiv \epsilon_{wall}/(1 + 0.24R_e/L)$ as can be seen in figure 14(b). Using the same convention, we present the dependence of the cumulant on the surface interaction strength for various system sizes in the inset of the figure. The cumulants depend monotonically on ϵ'_{wall} and exhibit a common intersection point around $\epsilon'^{crit}_{wall}/k_BT \approx 0.033\,15$.

This common intersection point as well as the monotonic behaviour as a function of the surface interactions is expected for a second order transition [84], and the behaviour of the cumulant significantly differs from the behaviour at the lower temperature (see figure 13 inset). In figure 15 we additionally present the probability distribution of the composition ϕ at this intersection point: the distribution is bimodal and the largest system sizes collapse onto a master curve without any size-dependent pre-factor. Therefore we conclude that the interface

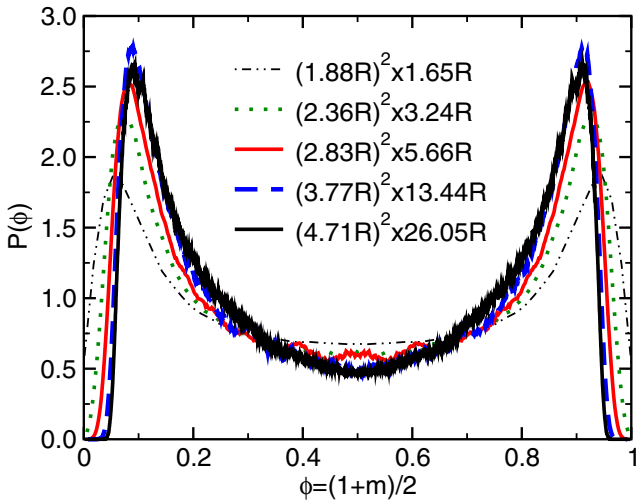

Figure 15. Scaling of the probability distribution $\mathcal{P}(\phi)$ at our estimate of the critical point, $\epsilon_{\text{wall}}/k_{\text{B}}T = 0.033\,15(1 + 0.24R_{\text{e}}/L)$, and various system sizes ranging from 28 000 to 2828 800 lattice sites.

localization/delocalization transition is of second order[3] although the wetting transition on a planar surface at $\epsilon/k_{\text{B}}T = 0.025$ is of first order.

Intriguingly there are also marked differences between this second order transition in an antisymmetric double wedge and the second order transition in a thin film which belongs to the two-dimensional Ising universality class. In the latter case, only the distribution of the *scaled* order parameter $L^{\beta/\nu}m$, where $\beta = 1/8$ and $\nu = 1$ are the critical exponents of the order parameter and the correlation length of the two-dimensional Ising universality class, exhibits data collapse for different system size. Moreover, as shown in figure 14, curves of the absolute value of the order parameter for different system sizes exhibit a common intersection point which agrees well with the intersection point of the cumulants. The analogous curves for an Ising model do not exhibit a common intersection point but monotonically converge towards $\langle|m|\rangle \sim |T - T_{\text{c}}|^{\beta}$ for $T < T_{\text{c}}$ and $\langle|m|\rangle \equiv 0$ for $T \geqslant T_{\text{c}}$ upon increasing the system size.

To relate the critical behaviour of the antisymmetric double wedge to the predictions of Parry *et al* [82], we regard the distance l_0 of the AB interface from the corner of one wedge. Similarly to an antisymmetric film (see section 4.1), we assume that we can approximate the distribution in a double wedge by the superposition of the distributions of single wedges $P_{\text{wedge}}(l_0)$ via $P(l_0) \sim P_{\text{wedge}}(l_0) + P_{\text{wedge}}(\sqrt{2}L - l_0)$. If the two distributions $P_{\text{wedge}}(l_0)$ and $P_{\text{wedge}}(\sqrt{2}L - l_0)$ do not overlap, the AB interface will be located in either of the two wedges and the order parameter will not vanish. If the two distributions overlap, the interface fluctuates around the diagonal and the order parameter will be zero. Right at the transition the two distributions begin to overlap:

$$\langle l_0\rangle + \xi_{\perp} \stackrel{!}{=} \sqrt{2}L - \langle l_0\rangle - \xi_{\perp} \qquad \text{(interface localization/delocalization in double wedge)} \tag{21}$$

[3] The interface localization/delocalization transition might be of second order in a very thin antisymmetric film (see section 4.2) even if the wetting transition is of first order. Therefore still larger system sizes would be desirable to confirm this conclusion. We note, however, that the thickness of the enrichment layer at the first order wetting transition of the planar substrate ($\epsilon/k_{\text{B}}T = 0.0226$, $\epsilon^{\text{wet}}_{\text{wall}}/k_{\text{B}}T = 0.04$) is only $l_0 \approx 0.24R_{\text{e}} \ll 3.33R_{\text{e}} = L/\sqrt{2}$. Therefore we believe that our conclusion is not affected by finite size effects.

where $\langle l_0 \rangle$ denotes the mean height in a single wedge and $\xi_\perp$ its fluctuations. Importantly, Parry's prediction of $\beta_0 = \nu_\perp$ in wedges (and also corners [85]) means that the height and its fluctuations are of the same order. They diverge as we approach the critical filling transition.

The height of the interface l_0 is related to the order parameter m of the localization/delocalization transition. Therefore we expect the distribution of the order parameter also to be bimodal. As $l_0 \sim \xi \sim L$ at the transition and the order parameter is a function of l_0/L, the distribution of the order parameter will exhibit two peaks whose positions and widths will not depend on the system size. This is exactly what we observe in figure 15. Using this observation and the standard finite size scaling assumption at a second order phase transition

$$P(m) \sim L^{\beta/\nu_\perp} \tilde{\mathcal{P}}(L^{\beta/\nu_\perp} m, L/\xi_\perp, L_y/\xi_y) \sim L^{\beta/\nu_\perp} \mathcal{P}(L^{\beta/\nu_\perp} m, L^{1/\nu_\perp} t, \eta) \quad (22)$$

where $\tilde{\mathcal{P}}$ and $\mathcal{P}$ are scaling functions, $t = (T - T_f)/T_f$ denotes the relative distance to the filling transition, and $\eta \equiv L_y/L^{\nu_y/\nu_\perp} = L_y/L^3$ denotes the generalized aspect ratio, we conclude that $\beta/\nu_\perp = 0$. Due to the anisotropy of the fluctuations of the interface along the wedge with correlation length ξ_y and perpendicular to the wedge with correlation length $\xi_\perp$, the generalized aspect ratio appears as a scaling variable. In our simulations we have chosen the system geometry such that η remains approximately constant, $\eta = 8.6 \times 10^{-4}$, to ensure that the finite-size rounding in the direction along the wedge and the rounding in the two other directions sets in simultaneously[4]. Hence, the scaling of the probability distribution not only confirms $\beta = 0$ but also the ratio $\nu_y = 3\nu_\perp$.

Knowing the probability distribution of the order parameter we can calculate all of its moments:

$$\langle m^k \rangle = \mathcal{M}_k(L^{1/\nu_\perp} t, \eta) \quad (23)$$

where $\mathcal{M}_k$ are scaling functions. A consequence of the absence of any L-dependent prefactor in equation (23) is the common intersection of moments of the order parameter at the transition. Again this is in agreement with our observation in figure 13(b). As this intersection involves only the lowest moment of the order parameter it yields an accurate estimate of the location of the critical interface localization/delocalization transition in an antisymmetric double wedge. As a special case of equation (23), we calculate the susceptibility of the order parameter: $\chi = L^2 L_y \langle m^2 \rangle / k_B T \sim L^2 L_y \tilde{\mathcal{M}}_2(L/\xi_\perp, L_y/\xi_y) \sim \xi_\perp^2 \xi_y \sim t^{-2\nu_\perp - \nu_y} \equiv t^{-\gamma}$ with $\gamma = 2\nu_\perp + \nu_y = 5/4$. Gratifyingly, these values for the exponents comply with the anisotropic hyperscaling relation [86] $\gamma + 2\beta = (d-1)\nu_\perp + \nu_y$. Using thermodynamic scaling $2 - \alpha = \gamma + 2\beta$ we also infer the critical exponent $\alpha = 3/4$ for the specific heat.

The scaling behaviour of the susceptibility is shown in figure 16. By plotting the fluctuations $\langle m^2 \rangle - \langle |m| \rangle^2$ versus the scaling variable $L^{1/\nu_\perp}(\epsilon'_{\text{wall}} - \epsilon'^{\text{crit}}_{\text{wall}})$ we confirm the exponents $\beta = 0$ and $\nu_\perp = 1/4$. From the divergence upon approaching the critical point, we read off the exponent γ. The data for the localized branch ($\epsilon'_{\text{wall}} \to \epsilon'^{\text{crit+}}_{\text{wall}}$) are well compatible with the prediction $\gamma = 5/4$. Similarly to the simulations of Ising systems [22], however, it seems much more difficult to observe the critical exponent upon approaching the transition from the delocalized state. One reason for this difficulty is the rather small value of η and the rather broad critical distribution (see figure 15). The broadness of the distribution (i.e., the fact that the peaks are located close to $m = \pm 1$ or that the distance l_0 of the AB interface from the bottom of the wedge is a small, but finite, fraction of the system size L) implies that the AB interface in the localized state ($\epsilon'_{\text{wall}} < \epsilon'^{\text{crit}}_{\text{wall}}$) is closely bound to the bottom of the wedge and microscopic details become important for the system sizes accessible to MC simulations.

[4] If we kept the ratio L_y/L constant $\eta \to 0$ and the system would exhibit a behaviour characteristic of a corner. In the limit L fixed but $L_y \to \infty$ the wedge becomes quasi-one-dimensional and there is no transition [22].

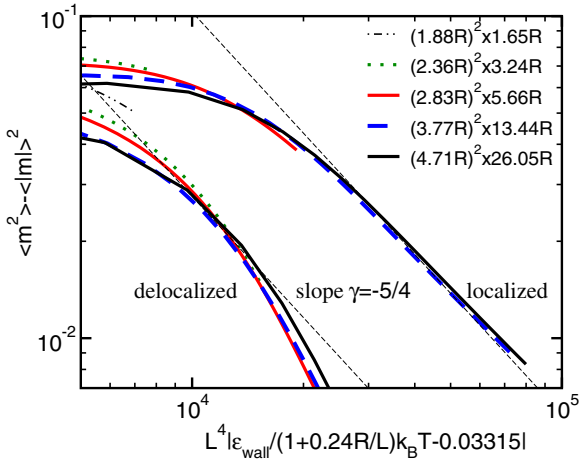

Figure 16. Scaling of the fluctuations of the order parameter. The data collapse corroborates the exponents $\beta = 0$ and $1/\nu_\perp = 4$. From the dependence of the susceptibility on the field one can estimate the exponent γ. The prediction $\gamma = 5/4$ is indicated by thin dashed lines.

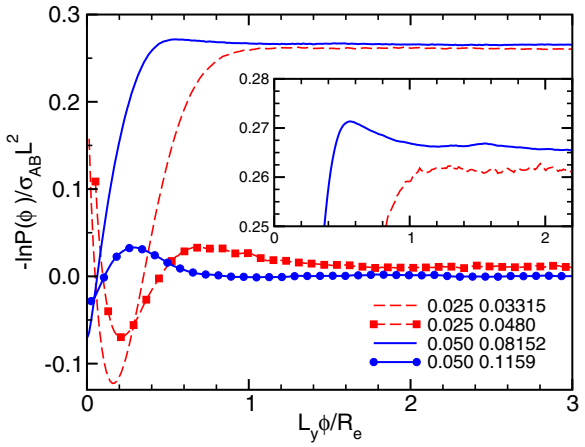

Figure 17. The probability distribution of the composition in an antisymmetric film with system geometry $2.8R_e \times 2.8R_e \times 5.6R_e$. The values of ϵ/k_BT and ϵ_{wall}/k_BT (shown in the key) correspond to the wetting transition and the filling transition (according to Young's equation).

It is interesting to relate the observation of first and second order interface localization/delocalization transitions in a double wedge to the shape of the interface potential. Parry *et al* predict [82] that the filling transition is second order if the interface potential between an AB interface and a planar surface does not exhibit a free energy barrier between the minimum close to the surface and the behaviour at large distances, i.e., if a macroscopically thick layer is not even metastable.

In figure 17 we present the interface potential obtained from the probability distribution of the composition in a simulation of an antisymmetric film at $\epsilon/k_BT = 0.025$. In the vicinity of the wetting transition the interface potential exhibits a maximum between the minimum close to the surface and the value at large distances. This fact confirms that the wetting transition is of first order. At the smaller value of ϵ_{wall}, however, there is no such maximum within the

statistical uncertainty of the MC data and, in agreement with Parry's predictions, we observe a second order transition in the double wedge.

6. Summary

We have investigated the interplay between wetting and phase separation of incompressible binary mixtures confined in thin films and wedges. In our polymer model, the wetting transition if of first order, and we can accurately locate it via Young's equation [14]. The concomitant pre-wetting behaviour modifies the phase boundaries in thin films [13]. If both surfaces attract the same component, capillary condensation occurs, and the critical point is close to the critical unmixing transition in the bulk. If one surfaces attracts the A-component but the other attracts the B-component an interface localization/delocalization transition occurs. In this case there are two critical points which correspond to the pre-wetting critical points at each surface. If the film width is very small, however, the interface localization/delocalization transition might be of second order even if the wetting transition is of first order. The critical points in a thin film are characterized by Ising critical behaviour.

In analogy to the interface localization/delocalization in an antisymmetric film, we have studied the transition in an antisymmetric double wedge and we relate the phase behaviour to the filling transition in a single wedge. Importantly we present evidence that the analogy of critical filling in an antisymmetric double wedge geometry gives rise to unconventional critical behaviour characterized by an order parameter exponent $\beta = 0$ and strong anisotropic fluctuations [22]. We can relate the critical exponents to the predictions of Parry *et al* [82] on critical filling. In agreement with those predictions, the filling transition can be critical even though the wetting transition on a planar substrate is of first order. This is practically important because there is no experimental realization of critical wetting on a solid substrate. Our findings suggests the polymer blends might be promising candidates for exploring the wetting and filling behaviour experimentally.

Acknowledgments

It is a great pleasure to thank E V Albano, D P Landau and A Milchev for fruitful collaborations and J M Romero-Enrique, S Dietrich, A O Parry for stimulating discussions. Financial support by the DFG under grants Bi314/17 (1-3) within the priority program 'Wetting and structure formation at interfaces', Mu 1674/1-1 (Heisenberg fellowship), and DAAD/PROALAR 2000 as well as computer time at NIC Jülich and HLR Stuttgart are acknowledged.

References

[1] Dietrich S 1988 *Phase Transitions and Critical Phenomena* vol 12, ed C Domb and J Lebowitz (London: Academic)
[2] Schick M 1990 *Liquids at Interfaces* ed J Charvolin, J F Joanny and J Zinn-Justin (Amsterdam: North-Holland) p 415
[3] Evans R 1990 *J. Phys.: Condens. Matter* **2** 8989
[4] Parry A O 1996 *J. Phys.: Condens. Matter* **8** 10761
[5] Fisher M E and Nakanishi H 1981 *J. Chem. Phys.* **75** 5857
Nakanishi H and Fisher M E 1983 *J. Chem. Phys.* **78** 3279
[6] Gelb L D, Gubbins K E, Radhakrishnan R and Sliwinska-Bartkowiak M 1999 *Rep. Prog. Phys.* **62** 1573
[7] Binder K, Landau D L and Müller M 2003 *J. Stat. Phys.* **110** 1411
[8] Rysz J, Budkowski A, Bernasik A, Klein J, Kowalski K, Jedlinski J and Fetters L J 2000 *Europhys. Lett.* **50** 35
[9] Geoghegan M, Ermer H, Jüngst G, Krausch G and Brenn R 2000 *Phys. Rev.* E **62** 940

[10] Müller-Buschbaum P 2003 *J. Phys.: Condens. Matter* **15** R1549
[11] Müller-Buschbaum P, VanHorne P, Scheumann V and Stamm M 1993 *Europhys. Lett.* **40** 655
Müller M, MacDowell L G, Müller-Buschbaum P, Wunnike O and Stamm M 2001 *J. Chem. Phys.* **115** 9960
[12] Müller M, Binder K and Albano E V 2000 *Europhys. Lett.* **49** 724
[13] Müller M, Albano E V and Binder K 2000 *Phys. Rev.* E **62** 5281
Müller M, Binder K and Albano E V 2000 *Physica* A **279** 188
[14] Müller M and Binder K 1998 *Macromolecules* **31** 8323
[15] Müller M and Binder K 2001 *Phys. Rev.* E **63** 021602
[16] Müller M, Binder K and Albano E V 2001 *Int. J. Mod. Phys.* B **15** 1867
[17] Müller M 1999 *Macromol. Theory Simul.* **8** 343
[18] Ginzburg V L 1960 *Sov. Phys.—Solid State* **1** 1824
de Gennes P G 1977 *J. Physique Lett.* **38** L-441
Joanny J F 1978 *J. Phys. A: Math. Gen.* **11** L-117
Binder K 1984 *Phys. Rev.* A **29** 341
[19] Composto R J, Walters R M and Genzer J 2002 *Mater. Sci. Eng. Rep.* **38** 107
[20] Geoghegan M and Krausch G 2003 *Prog. Polym. Sci.* **28** 261
[21] Carmesin I and Kremer K 1988 *Macromolecules* **21** 2819
Deutsch H-P and Binder K 1991 *J. Chem. Phys.* **94** 2294
[22] Milchev A, Müller M, Binder K and Landau D P 2003 *Phys. Rev. Lett.* **90** 131601
[23] Milchev A, Müller M, Binder K and Landau D P 2003 *Phys. Rev.* E **68** 031601
[24] Konynenburg P H and Scott R L 1980 *Phil. Trans. R. Soc.* A **298** 496
[25] MacDowell L G, Virnau P, Müller M and Binder K 2002 *J. Chem. Phys.* **117** 6360
Müller M, MacDowell L G, Virnau P and Binder K 2002 *J. Chem. Phys.* **117** 5480
[26] Müller M 2002 *Comput. Phys. Commun.* **147** 292
[27] Lin Y-C, Müller M and Binder K 2004 *J. Chem. Phys.* **121** 3816
Morita H, Kawakatsu T and Doi M 2001 *Macromolecules* **34** 8777
[28] Dalnoki-Veress K, Forrest J A and Dutcher J R 1999 *Phys. Rev. Lett.* **82** 1486
Dalnoki-Veress K, Forrest J A and Dutcher J R 1998 *Phys. Rev.* E **57** 5811
[29] Müller M, Katsov K and Schick M 2003 *J. Polym. Sci.* B **41** 1441
Müller M, Katsov K and Schick M 2003 *Biophys. J.* **85** 1611
Müller M, Katsov K and Schick M 2002 *J. Chem. Phys.* **116** 2342
[30] Sariban A and Binder K 1988 *Macromolecules* **21** 711
Sariban A and Binder K 1987 *J. Chem. Phys.* **86** 5859
[31] Müller M 1995 *Macromolecules* **28** 6556
[32] Müller M and Binder K 1995 *Macromolecules* **28** 1825
[33] Müller M and Schick M 1996 *J. Chem. Phys.* **105** 8885
[34] Borgs C and Kotecky R 1990 *J. Stat. Phys.* **60** 79
Borgs C and Kotecky R 1992 *Phys. Rev. Lett.* **68** 1734
[35] Berg B A and Neuhaus T 1992 *Phys. Rev. Lett.* **68** 9
Berg B A, Hansmann U and Neuhaus T 1993 *Z. Phys.* B **90** 229
[36] Ferrenberg A M and Swendsen R 1988 *Phys. Rev. Lett.* **61** 2635
[37] Wang F and Landau D P 2001 *Phys. Rev. Lett.* **86** 2050
[38] Virnau P and Müller M 2004 *J. Chem. Phys.* **120** 10925
[39] Binder K 1982 *Phys. Rev.* A **25** 1699
[40] Müller M and MacDowell L G 2000 *Macromolecules* **33** 3902
[41] Müller M and MacDowell L G 2003 *J. Phys.: Condens. Matter* **15** R609
[42] Müller M, MacDowell L G and Yethiraj A 2003 *J. Chem. Phys.* **118** 2929
[43] Helfand E and Tagami Y 1972 *J. Chem. Phys.* **56** 3592
[44] Noolandi J and Hong K M 1981 *Macromolecules* **14** 727
[45] Matsen M W and Schick M 1994 *Phys. Rev. Lett.* **72** 2660
[46] Geisinger T, Müller M and Binder K 1999 *J. Chem. Phys.* **111** 5241
Matsen M W 1997 *J. Chem. Phys.* **106** 7781
[47] Lifshitz I M 1978 *Rev. Mod. Phys.* **50** 683
[48] Edwards S F 1965 *Proc. Phys. Soc.* **85** 613
[49] Nakanishi H and Pincus P 1983 *J. Chem. Phys.* **79** 997
[50] Schmidt I and Binder K 1985 *J. Physique* **46** 1631
[51] Flebbe T, Dünweg B and Binder K 1996 *J. Physique* II **6** 667
[52] Freed K F 1996 *J. Chem. Phys.* **105** 10572

[53] Cohen S M and Muthukumar M 1989 *J. Chem. Phys.* **90** 5749
[54] Jerry R A and Nauman E B 1992 *J. Chem. Phys.* **97** 7829
[55] Reister E and Müller M 2003 *J. Chem. Phys.* **118** 8476
[56] Reister E, Müller M and Binder K 2001 *Phys. Rev.* E **64** 041804
[57] Müller M and Schmid F 2004 *Adv. Polym. Sci.* at press
[58] Hohenberg P C and Halperin B I 1977 *Rev. Mod. Phys.* **49** 435
[59] de Gennes P G 1980 *J. Chem. Phys.* **72** 4756
Pincus P 1981 *J. Chem. Phys.* **75** 1996
Binder K 1983 *J. Chem. Phys.* **79** 6387
[60] Maurits N M and Fraaije J G E M 1997 *Chem. Phys.* **107** 5879
[61] Semenov A N 1996 *J. Physique* II **6** 1759
[62] Young T 1805 *Phil. Trans. R. Soc.* **95** 65
[63] Carmesin I and Noolandi J 1989 *Macromolecules* **22** 1689
[64] MacDowell L G, Müller M and Binder K 2002 *Colloids Surf.* A **206** 277
[65] Reister E, Müller M and Kumar S K 2004 in preparation
[66] Nicolaides D and Evans R 1989 *Phys. Rev.* B **39** 9336
Evans R and Marconi U M B 1985 *Phys. Rev.* A **32** 3817
[67] Brochard-Wyart F and de Gennes P-G 1983 *C. R. Acad. Sci. Paris* **297** 223
[68] Parry A O and Evans R 1990 *Phys. Rev. Lett.* **64** 439
Parry A O and Evans R 1992 *Physica* A **181** 250
[69] Binder K, Landau D P and Ferrenberg A M 1995 *Phys. Rev.* E **51** 2823
Albano E V, Binder K, Heermann D W and Paul W 1989 *Surf. Sci.* **233** 151
[70] Swift M R, Owczarek A L and Indekeu J O 1991 *Europhys. Lett.* **14** 475
[71] Wilding N B and Nielaba P 1996 *Phys. Rev.* E **53** 926
[72] Parry A O and Boulter J C 1995 *Physica* A **218** 77
Parry A O and Boulter J C 1995 *Physica* A **218** 109
[73] Fisher M E and Jin A J 1992 *Phys. Rev. Lett.* **69** 792
Jin A J and Fisher M E 1993 *Phys. Rev.* B **47** 7365
[74] Werner A, Schmid F, Müller M and Binder K 1997 *J. Chem. Phys.* **107** 8175
[75] Müller M and Werner A 1997 *J. Chem. Phys.* **107** 10764
[76] Fisher D S and Huse D A 1985 *Phys. Rev.* B **32** 247
[77] Fisher M E and Wen H 1992 *Phys. Rev. Lett.* **68** 3645
[78] Lipowsky R, Kroll D M and Zia R K P 1983 *Phys. Rev.* B **27** 499
[79] Brezin E, Halperin B I and Leibler S 1983 *Phys. Rev. Lett.* **50** 1387
[80] Fredrickson G H and Bates F S 1997 *Polym. Sci.* B **35** 2775
Jeon H S, Lee J H and Balsara N P 1997 *Phys. Rev. Lett.* **79** 3274
Morkved T L, Chapman B R, Bates F S, Lodge T P, Stepanek P and Almdal K 1999 *Faraday Discuss.* **11** 335
[81] Düchs D, Ganesan V, Fredrickson G H and Schmid F 2003 *Macromolecules* **36** 9237
[82] Parry A O, Rascon C and Wood A J 1999 *Phys. Rev. Lett.* **83** 5535
[83] Rejmer K, Dietrich S and Napiorkowski M 1999 *Phys. Rev.* E **60** 4027
[84] Binder K 1981 *Z. Phys.* B **43** 119
Binder K 1981 *Phys. Rev. Lett.* **47** 693
[85] Albano E V, de Virgiliis A, Müller M and Binder K 2003 *J. Phys.: Condens. Matter* **15** 333
[86] Binder K and Wang J S 1989 *J. Stat. Phys.* **55** 87